PERFORMANCE BASED ASSESSMENT OF NUMBER OF EQUIVALENT UNIFORM CYCLIC STRESS SCHEME

A THESIS SUBMITTED TO
THE GRADUATE SCHOOL OF NATURAL AND APPLIED SCIENCES
OF
MIDDLE EAST TECHNICAL UNIVERSITY

BY

ERAY ALTINCI

IN PARTIAL FULFILLMENT OF THE REQUIREMENTS
FOR
THE DEGREE OF MASTER OF SCIENCE
IN
CIVIL ENGINEERING

NOVEMBER 2019

Approval of the thesis:

PERFORMANCE BASED ASSESSMENT OF NUMBER OF EQUIVALENT UNIFORM CYCLIC STRESS SCHEME

submitted by **ERAY ALTINCI** in partial fulfillment of the requirements for the degree of **Master of Science in Civil Engineering Department, Middle East Technical University** by,

Prof. Dr. Halil Kalıpçılar
Dean, Graduate School of **Natural and Applied Sciences** _____

Prof. Dr. Ahmet Türer
Head of Department, **Civil Engineering** _____

Prof. Dr. Kemal Önder Çetin
Supervisor, **Civil Engineering, METU** _____

Examining Committee Members:

Prof. Dr. Erdal Çokça
Civil Engineering, METU _____

Prof. Dr. Kemal Önder Çetin
Civil Engineering, METU _____

Prof. Dr. Zeynep Gülerce
Civil Engineering, METU _____

Assoc. Prof. Dr. Kartal Toker
Civil Engineering, METU _____

Prof. Dr. Nihat Sinan Işık
Civil Engineering, Gazi University _____

Date: 29.11.2019

I hereby declare that all information in this document has been obtained and presented in accordance with academic rules and ethical conduct. I also declare that, as required by these rules and conduct, I have fully cited and referenced all material and results that are not original to this work.

Name, Surname:Eray Altıncı

Signature:

ABSTRACT

PERFORMANCE BASED ASSESSMENT OF NUMBER OF EQUIVALENT UNIFORM CYCLIC STRESS SCHEME

Altıncı, Eray
Master of Science, Civil Engineering
Supervisor: Prof. Dr. Kemal Önder Çetin

November 2019, 82 pages

Assessment of cyclic (seismic) response of soils is considered to be one of the most interesting research areas of geotechnical engineering. Cyclic loading-induced stresses cause accumulation of shear strains and generation of excess pore water pressure, which are accompanied by reduction in stiffness. In the most extreme cases, this process leads to soil liquefaction. As opposed to the random nature of earthquake waves, it is generally preferred to apply uniform loading cycles to undisturbed or reconstituted soil samples in the laboratory. The method proposed by Seed et al. (1975) can be used to convert the acceleration time history to number of equivalent uniform stress cycles. This approach uses a weighting factor, which varies as a function of selected failure criterion (Cetin and Bilge, 2012), and allows direct calculation. The aim of this study is to develop a new semi-empirical framework to predict number of equivalent stress cycles. For this purpose, more than 4000 acceleration time histories from PEER database with different magnitudes, site-source distance and site types have been assessed. These records were filtered and re-sampled to a common time step, and then the number of uniform cycles was calculated for 17 different weighting factors ranging from 0.2 to 1.0 to form a database. This database was assessed by regression methods to develop a probability-based model for

prediction the number of equivalent uniform stress cycles for a given earthquake magnitude, site-source distance, soil properties and selected cyclic target strain performance criterion.

Keywords: Seismic soil response, Number of equivalent uniform stress cycles, Probabilistic methods

ÖZ

EŞDEĞER ÇEVRİMSEL GERİLME SAYISININ PERFORMANSA DAYALI BELİRLENMESİ

Altıncı, Eray
Yüksek Lisans, İnşaat Mühendisliği
Tez Danışmanı: Prof. Dr. Kemal Önder Çetin

Kasım 2019, 82 sayfa

Zeminlerin çevrimsel (sismik) yükler altındaki davranışlarının incelenmesi geoteknik mühendisliğinin en dikkat çekici araştırma alanlarındandır. Deprem sırasında meydana gelen çevrimsel gerilmeler, zemin danelerinin kayma birim deformasyonlarına maruz kalmasına, buna bağlı boşluk suyu basıncı artışına ve zeminde rijitliğinin kaybına neden olmaktadır. En uç durumda sıvılaşma tetiklenmesine neden olacak bu süreç neden olduğu dramatik sonuçlar nedeniyle birçok araştırmanın odağı olmuştur. Deprem dalgalarının düzensiz doğasına karşın laboratuvar deneylerine dayalı çalışmalarda, örselenmemiş zemin numunesi veya hazırlanan örneğe genellikle düzenli çevrimsel yük uygulanır. Değerlendirilmek istenen düzensiz ivme – zaman kaydının eşdeğer çevrim sayısına çevrilmesi için Seed vd. (1975) tarafından önerilen yöntem kullanılabilir. Bu yöntem seçilen yenilme kriterine bağlı olarak değiştiği bilinen bir ağırlık faktörüne (Cetin ve Bilge, 2012) bağlı olup doğrudan hesap yapılmasına olanak tanımaktadır. Bu çalışma kapsamında ise eşdeğer düzenli çevrimsel gerilme sayısının belirlenmesine yönelik bir yarı-görgül yöntem geliştirilmesi hedeflenmiştir. Bu amaçla, PEER kataloğunda yer alan, farklı deprem büyüklüğü, kaynak mesafesi ve saha tipine sahip 4000'in üzerinde kayıt değerlendirilmiştir. Kayıtlar filtrelenip, ortak bir zaman aralığında toplamak üzere

yeniden örneklendikten sonra, 0.2 ile 1.0 arasında değişen 17 farklı ağırlık faktörü için Seed vd. (1975) yöntemi uyarınca eşdeğer çevrim sayısı hesaplanarak bir veri tabanı oluşturulmuştur. Bu veri, olasılıksal yöntemlerle değerlendirilmiş, ardından deprem büyüklüğü, kaynağa mesafe, saha zemin özellikleri ve seçilen performans kriterine göre eşdeğer çevrim sayısının hesaplanmasına olanak tanıyan bir ifade geliştirilmiştir.

Anahtar Kelimeler: Sismik zemin davranışı, Eşdeğer düzenli çevrimsel gerilme sayısı, Olasılıksal yöntemler

To Dr. Kaan Erol, R.I.P….

To my family…

ACKNOWLEDGEMENTS

I would like to express my grateful appreciation to my supervisor Prof. Dr. Kemal Önder Çetin for his guidance, encouragement, patience and support at each step of this thesis. This work cannot be completed without his guidance, support and patience.

I would like to express my gratitude to Dr. Habib Tolga Bilge for his support and guidance in both this thesis and my professional career.

I would like to express my deep appreciation to Gürkan Tamer and Osman Canpolat. Thank you for being brothers to me.

I would also like to thank my mother Sönmez Altıncı and my father Ünal Altıncı for their support and unconditional love for me at every moment of my life. Without their love and support, I couldn't be who I am now.

TABLE OF CONTENTS

LIST OF TABLES

TABLES

LIST OF FIGURES

FIGURES

LIST OF SYMBOLS

SYMBOLS

$\Delta\sigma$	Stress drop
$\Delta\sigma^*$	Stress drop index
$\mu_{residual}$	Mean value of residuals
CSR	Cyclic stress ratio
D_R	Relative density
D_{source}	Theoretical seismic source
f_c	Corner frequency
g	Acceleration of gravity
GMPE	Ground motion prediction equations
γ_{max}	Maximum shear strain
m	Weighting factor
M_0	Moment magnitude in dyno-cm
MSF	Magnitude scaling factor
M_w	Moment magnitude
N	Number of equivalent uniform stress cycle
PGA	Peak ground acceleration
θ	Unknown model coefficients
r	Closest distance to the rupture plane
R_{jb}	Joyner-Boore distance
r_c	Cut off distance
$V_{s,30}$	Representative shear wave velocity of the top 30 m
B	Shear wave velocity at the source
E	Model uncertainty
$\sigma_{residual}$	Standard deviation of residuals
$\sigma'_{v,0}$	Vertical effective stress

CHAPTER 1

INTRODUCTION

1.1. Research Statement

Assessment of cyclic (seismic) response of soils is considered to be one of the most challenging topics in geotechnical engineering. Cyclic-induced stresses cause accumulation of shear strains and generation of excess pore water pressure, which are accompanied by reduction in stiffness. In the most extreme case, this process leads to soil liquefaction and many researchers have focused on this phenomenon considering its dramatic consequences. While some of these researchers used earthquake case histories, many others preferred using experimental data. In the latter approach, as opposed to the random and irregular nature of earthquake waves, cyclic loading is generally applied in a uniform manner (in the form of sine waves) to the reconstituted (or undisturbed) soil samples. Seed et al. (1975) proposed a method to represent an irregular stress time history by equivalent uniform stress series. Within the scope of this research, more than 4,000 acceleration time histories were compiled from PEER ground motion database and each record's equivalent number of stress cycles was determined by following Seed et al. (1975) method (Figure 1.1 schematically represents how number of equivalent uniform stress cycles vary for different weighting factors for a given acceleration time history) to compile a database in terms of related descriptive parameters (moment magnitude, site type, source-to-side distance, Seed et al.'s weighting factor, etc.). Based on this data, a robust probability-based semi-empirical model was developed to predict equivalent number of stress cycles of a scenario event defined by earthquake magnitude, distance to source mechanism, soil properties and selected performance (or failure) criterion.

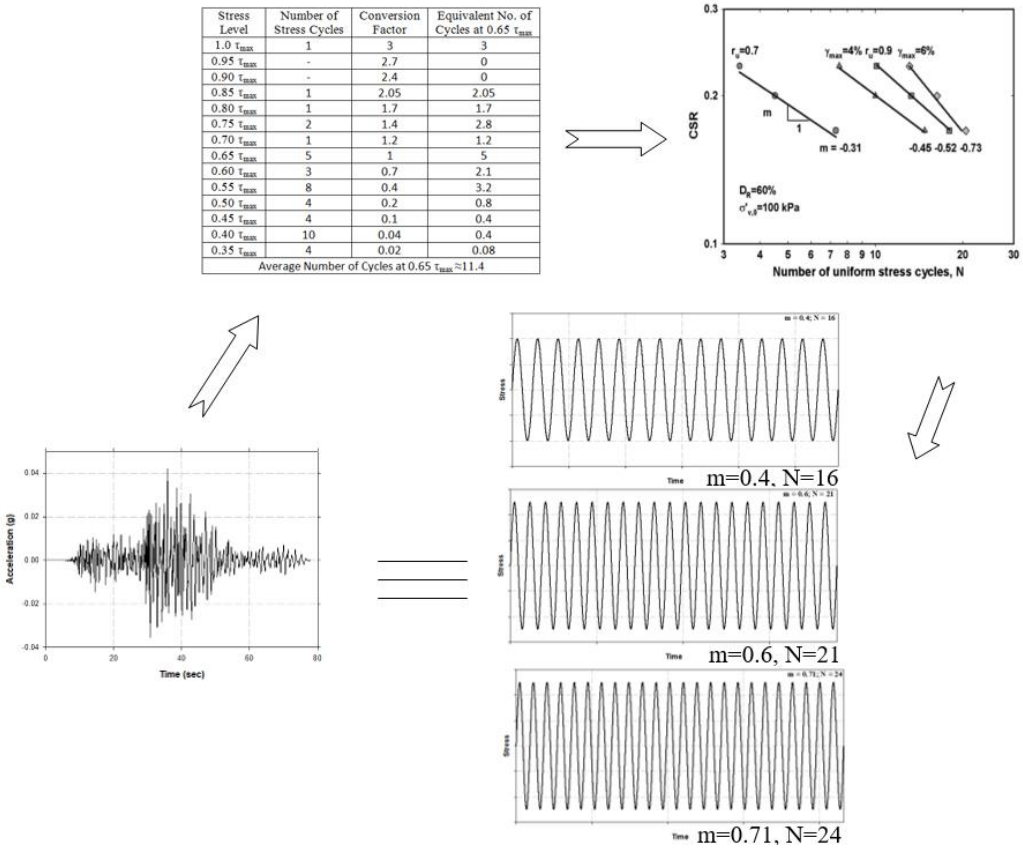

Figure 1.1. Schematic representation of number of cycle counting concept for different weighting factors

1.2. Problem Significance and Limitations of the Existing Studies

Considering its relation with intensity and duration of strong ground motions, earthquake magnitude is considered to be a vital parameter for geotechnical earthquake engineering assessments. While case history based approaches can directly use magnitude as a measure of duration, it is necessary to convert the magnitude to an applicable duration parameter in laboratory testing based approaches. Thus, robust methods for converting, mostly earthquake magnitude-dependent duration parameter, to equivalent uniform (harmonic) stress cycles, are needed. After these conversions, it is possible to have a more systematic and fair comparison between seismic resistance measured by laboratory tests under uniform cyclic loading conditions and field

conditions for which loading is irregular in nature. Hopefully, such comparisons will lead to the cross-calibration of laboratory and field test methods.

More than 4 decades have passed from the pioneering study of Seed et al. (1975). While the earliest efforts are mostly judgmental, in time more sophisticated approaches have been proposed. However, a critical review of the existing literature has revealed that; i) currently, a significantly extended ground motion database exists, enabling better assessment of cyclic stress conversions of irregular transient earthquake records to harmonic uniform stress cycles, and ii) based on the argument proposed by Cetin and Bilge (2012), weighting factor of conversion relationships are now known to be strain dependent. Hence, a revisit to the whole concept is needed. Inspired by these studies, it is aimed to develop a semi-empirical model for estimation of equivalent number of uniform stress cycles as a function of earthquake, site and performance parameters.

1.3. Definition of Soil Liquefaction

The model will also be used to develop magnitude scaling factor (MSF) which is related with soil liquefaction resistance. Under cyclic loading (e.g. earthquake, wave motion), accumulated shear strains and generated pore water pressure due to increase in cyclic-induced stresses cause liquefaction. This means, liquefaction is a type of soil behavior under cyclic loading that causes significant reduction in stiffness and shear strength. Bearing capacity failure and excessive settlement problems are most common failure types due to these reductions.

After two damaging 1964 Niigata – Japan (Figure 1.1) and 1964 Great Alaskan Earthquakes (Figure 1.2), engineering studies about liquefaction began to see interest quickly and liquefaction was defined differently by many researchers. Marcuson (1978) defined liquefaction as reduction in effective stress due to increase in pore-water pressure leads to transformation from solid to liquefied state of granular material.

*Figure 1.2.*Foundation failure by liquefaction after the 1964 Niigata Earthquake (Kramer and Elgamal 2001)

Figure 1.3. The 1964 Great Alaskan Earthquake (Hansen 1965)

Over the years, many improvements were performed in liquefaction engineering. Seed et al. 2003 pointed out "Today, the area of "soil liquefaction engineering" is emerging as a semi-mature field of practice in its own right. This area now involves a number of discernable sub-issues or sub-topics."

In liquefaction analyses, there are five common stages in evaluation of liquefaction problem. The first stage is checking that soil in field of study have liquefaction potential or not, and any cyclic motion that can trigger liquefaction will happen. After that, if the soils have a potential and any motion can trigger liquefaction in that soil can occur, then the next stage is assessment of strength and stability after liquefaction. The next stage is determination of expected deformations and displacements after earthquake. The fourth stage is assessment of consequences of these deformations and displacements. The last stage is design of remedial measures to reduce deformations and displacements, if necessary.

From the engineering view, factor of safety against liquefaction is evaluated simply calculating ratio of seismic demand and liquefaction resistance of soils. Laboratory testing is an alternative to determine the cyclic resistance. However, as mentioned in Cetin and Bilge (2012), using determined cyclic stress ratio and number of equivalent uniform stress cycle in laboratory for liquefaction analyses gives unsafe results due to limited practical use of laboratory liquefaction tests.

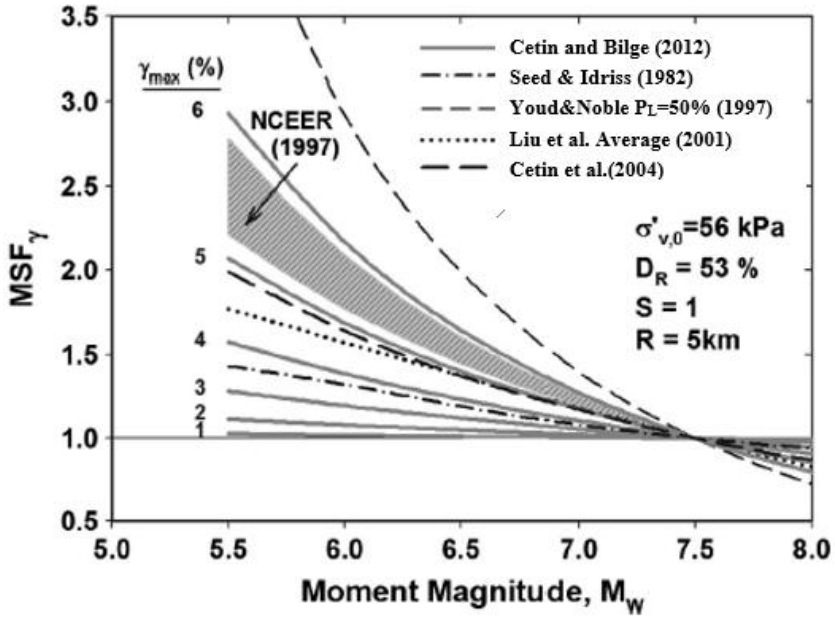

Figure 1.4. Comparison of Published strain based MSFs (Cetin and Bilge 2012)

Significant variations (about a factor of 3) in MSFs especially for earthquakes with relatively smaller magnitude (Figure 1.4) indicates the need to further study in this topic as recommended by Cetin and Bilge (2012). Due to variability of these suggested factors, effect of number of uniform stress cycle in liquefaction analyses were studied and number of uniform stress cycle started to serve as an effective parameter in liquefaction analyses. This study is performed to respond this need by developing a model to estimate number of equivalent uniform cyclic stress for different earthquake parameters and weighting factors.

1.4. Scope of the Thesis

Following this introduction, an overview of the available literature on equivalent number of cycle concept and existing approaches on its prediction will be presented in Chapter 2.

Chapter 3 is devoted to the compilation of database used for development of the proposed model.

Chapter 4 begins with the interpretation of existing trends of the database in terms of earthquake, site and performance parameters, and proceeds with a detailed presentation of the proposed probabilistically-based semi-empirical model for the assessment of equivalent number of uniform stress cycles.

Chapter 5 is devoted to comparative evaluation of the predictive performance of the proposed model and existing efforts by using some statistical measures.

Finally, a summary of the research, major conclusions, and recommendations for future studies are presented in Chapter 6.

CHAPTER 2

AN OVERVIEW OF EXISTING LITERATURE

2.1. Introduction

In their pioneering work, Seed et al. (1975) stated that the analytical procedures used for assessment of seismic liquefaction potential of soils involve determination of; i) cyclic shear stresses at different levels in the soil profile by ground response analysis or simplified procedure (Seed and Idriss, 1971), and ii) cyclic shear strength of soil for different confinement levels by performing laboratory tests. The simple representation of an irregular earthquake stress time history by a uniform series of stress cycles is a quite widely preferred approach in experimental studies. Liu et al. (2001) summarized the parameters required to describe a uniform series of stress cycles as; i) amplitude, ii) frequency and iii) number of cycles (N). While selection of amplitude and frequency content can be considered as more straight-forward, prediction of N remains as acritical issue. Within the confines of this section, the existing methods for prediction of N will be reviewed.

2.2. Previous Studies for Estimation of Number of Equivalent Uniform Cycle

In the earliest days of this research field, number of equivalent stress cycles had been estimated by judgment. Seed and Idriss (1971) have made their recommendations as a function of earthquake magnitude as presented in Table 2.1.

Table 2.1. *Typical N values for different magnitude earthquakes*

Magnitude	Equivalent Number of Uniform Stress Cycles, N
7	10
7.5	20
8	30

Later, Seed et al. (1975) proposed a more systematic approach for prediction number of equivalent stress cycles by adopting the weighting procedure defined by Lee and Chan (1972). In this approach, the effect of each cycle of an irregular loading pattern was given a weighting factor and the equivalent uniform stress cycle series was evaluated on this basis. Seed et al. (1975) mentioned that this weighting factor was determined based on laboratory test data. Later, Seed and Idriss (1982) used this concept while developing their first set of magnitude scaling (or duration weighting) factors. This weighting scheme is based on the observation that log (CSR) vs log (N) response is linear and the authors refer the slope of this line as their weighting factor (Figure 2.1). Seed et al. (1975) evaluated a total number of 57 earthquake acceleration time histories by using this approach and proposed a relation between earthquake magnitude (M_w) and equivalent uniform stress cycles (N). Later, Idriss (1997) repeated the same analyses by selecting a different weighting factor. The N – M_w correlations proposed by these researchers are presented in Figure 2.2.

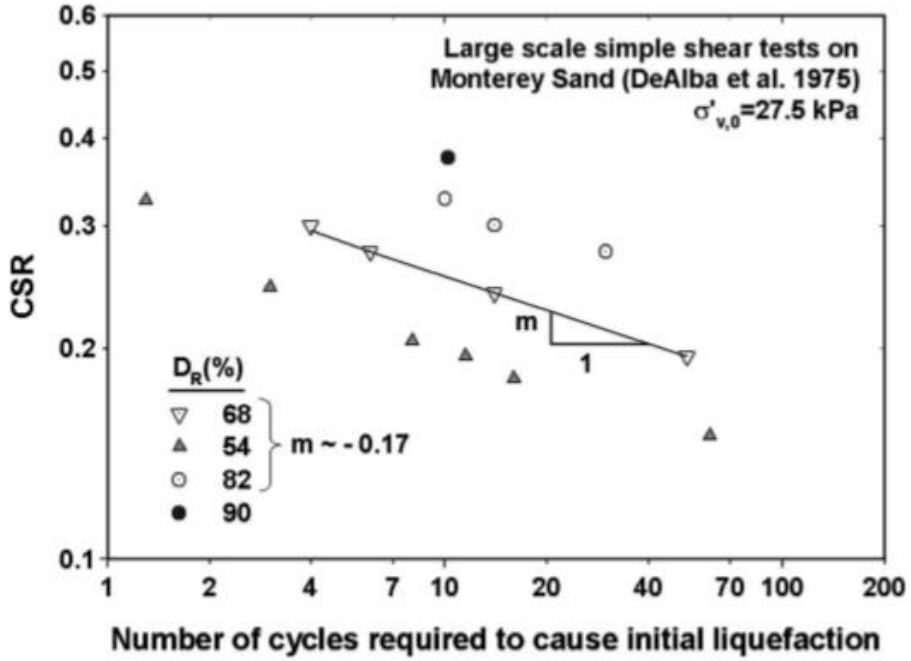

Figure 2.1. Large scale simple shear test results on Monterey Sand (DeAlba et al. 1975) (after Cetin and Bilge, 2012)

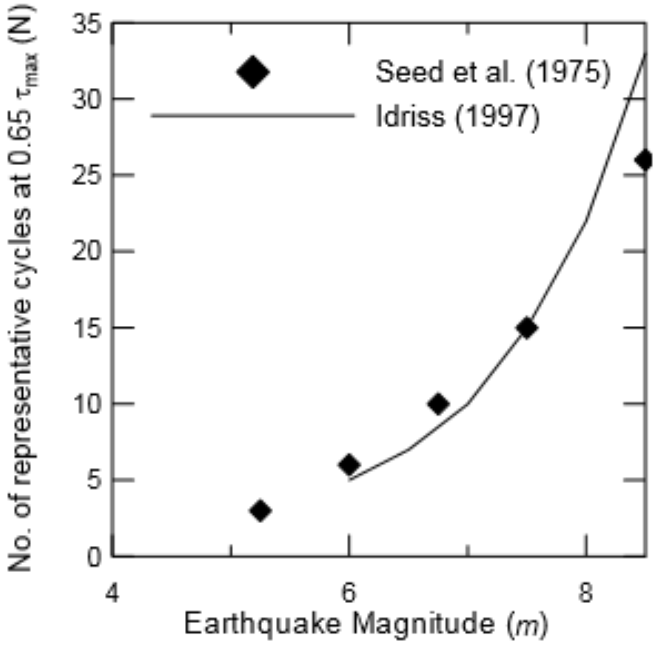

Figure 2.2. Relationships between N and M_w (after Liu et. al. 2001)

Although it was based on a very limited database, the recommendations of Seed et al. (1975) have served to the geotechnical earthquake engineering community for more than two decades. Later, Liu et al. (2001) developed empirical relationships between N and M_w, site – source distance (taken as the closest distance to the rupture plane), site conditions and factors representing near-fault rupture directivity effects. 1528 motion recordings from 107 earthquakes were used while developing these relationships. Earthquake dates range from the 1935 Helena, Montana, earthquake to the 1999 Duzce, Turkey, earthquake. Magnitudes (M_w) of these earthquakes range between4.7 and 7.6 with site-source distance (r) up to 200 km. Distribution of r and M_w of data used in that study is presented in Figure 2.3. Since time steps of these earthquake acceleration time histories are different from each other, they were decimated to a common time step of 0.02 seconds by first low-pass filtering the data with a corner frequency of 25 Hz (8^{th} order Chebyshev type I filter). Additional details about the data set were presented in Liu (2001).

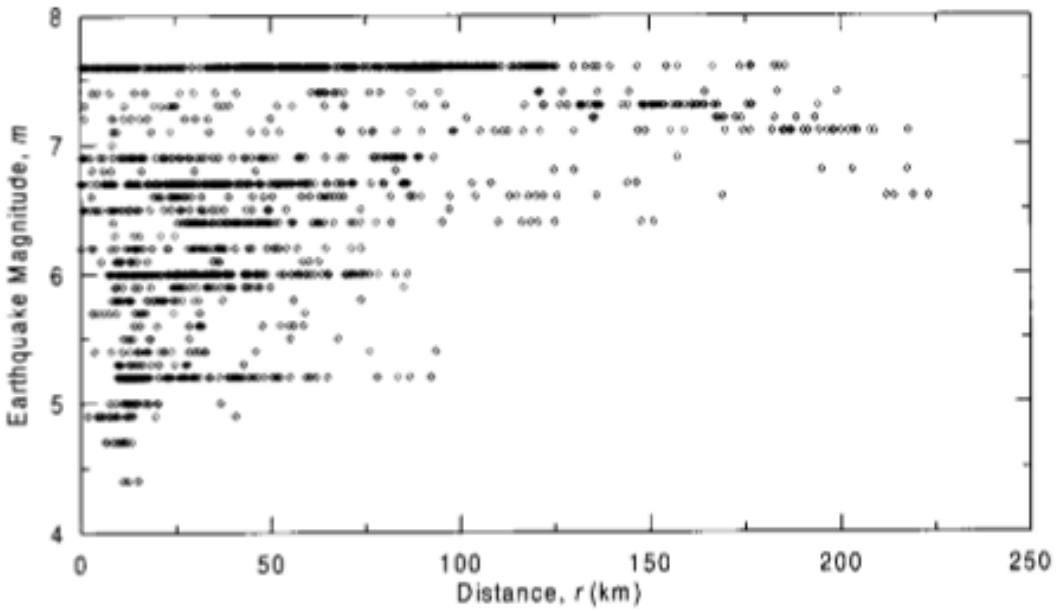

Figure 2.3. Distribution of data used in Liu (2001)

Within the scope of Liu (2001)'s study, irregular time history of earthquake induced cyclic stresses were converted to equivalent number of uniform stress cycles, N. This conversion consists of counting a number of local minimum and maximum points in a normalized accelerogram. This operation was performed in two steps. The first step was normalization of stress time histories and the second step was developing weighting factors. Shortly after Liu (2001), Liu et al. (2001) stated that N was evaluated by combining the two horizontal shaking components. Later, the data was probabilistically evaluated by using maximum likelihood method which enabled the estimation of both inter-event and intra-event standard errors. These components were combined to give the total standard error.

By following the trends existing in their database, Liu et al. (2001) developed an empirical model as a function of distance and site conditions for prediction of N. For the sake of completeness and the fact this study is one of the inspirations of this research; details of this model are presented in this chapter. Hanks and McGuire (1981) and Boore (1983) suggested that theoretical seismic source is inversely related to a corner frequency f_c in the Fourier amplitude source spectrum (Equation 2.1).

$$D_{source} = \frac{1}{f_c} \tag{2.1}$$

Brune (1970, 1971) has related f_c to the seismic moment and stress drop of a fault rupture as presented in Equation 2.2.

$$f_c = 4.9 * 10^6 \beta (\frac{\Delta\sigma}{M_0})^{1/3} \tag{2.2}$$

In Equation 2.2, β is the shear wave velocity at the source (generally taken as 3.2 km/s), Δσ is the stress drop in bars, and M_0 is the seismic moment (in dyne-cm). Liu (2001) determined N to be well correlated to significant duration with correlation coefficient ≈0.62. Accordingly, D_{source} is replaced with N in Equation 2.1. After this replacement, note that Δσ is not the same stress drop as Brune (1971) suggested. Therefore, Equation 2.2 and 2.1 are combined and updated (side effects were taken into account) as presented in Equation 2.3.

$$N = \frac{1}{f_c(M_0, \Delta\sigma *)} + f_1(r) + f_2(S, r) \tag{2.3}$$

In Equation 2.3, $f_1(r)$ is the distance factor and f_2 (S,r) is the site dependence factor where S=0 for rock sites, and S=1 for soil sites. The distance dependence factor as follows;

$$f_1(r) = 0; \qquad r < r_c \tag{2.4a}$$

$$f_1(r) = c_2(r - r_c); \qquad r \geq r_c \tag{2.4b}$$

where r_c is a cutoff distance in kilometers. In addition, a site dependence factor was suggested by Liu et al. (2001) as follows;

$$f_2(S, r) = c_1 S r < r_c (2.5a)$$

$$f_2(S, r) = S[c_1 + c_3(r - r_c)] r \geq r_c \tag{2.5b}$$

Hanks and Kanamori (1979) suggested a relationship between moment magnitude and seismic moment as $M_0 = 10^{1.5M+16.05}$ and replaced in the equation 2.3.

Three phases of regression analyses were performed by Liu et al. (2001) to determine the coefficients and these phases are summarized as follows.

1. Stress Drop Index Independent of Magnitude: First regression was performed by Liu et al. (2001) to determine stress drop index ($\Delta\sigma^*$), c_1, c_2, c_3 and r_c coefficients. After separate regressions were performed, c_3 term was dropped from the equation and r_c term was determined as zero.

2. Stress Drop Index as Function of Magnitude: After the first phase, c_3 and r_c terms were dropped from equation. Then, for different magnitude ranges, separate regression analyses were performed by Liu et al. (2001) to determine $\Delta\sigma^*$. According to determined $\Delta\sigma^*$ values for different magnitude ranges, an exponential model for stress drop index was developed as presented in Equation 2.6.

$$\Delta\sigma^* = \exp[b_1 + b_2(m - m^*)] \tag{2.6}$$

where reference magnitude, m^* was evaluated as 5.8 by regression, and for this value remaining coefficients were determined by Liu et al. (2001) as presented in Table 2.2.

3. Near - Fault Directivity Effects: Liu et al. (2001) mentioned that fault rupture directivity effect given by Somerville et al. (1997) was used in their study. To consider that effect, residual parameter (ε) was determined as a function.

After three phases of regression analyses, empirical relationship developed by Liu et al. (2001) to obtain N is presented in Equation 2.7 and estimated coefficients are presented in Table 2.2.

$$\ln(N) = ln\left[\frac{\left(\frac{\exp(b_1+b_2(m-m^*))}{10^{1.5m+16.05}}\right)^{-1/3}}{4.9*10^6\beta} + Sc_1 + rc_2\right] + \varepsilon \tag{2.7}$$

Within the scope of Liu et al. (2001), both field based and laboratory based weighting factors were used to calculate N values for all time histories. Calculated N values for field-based weighting factors were higher than laboratory based weighting factors.

Table 2.2. *Coefficients estimated by Liu et al. (2001)*

Coefficients	Estimate
(a) Laboratory – based weighting factors	
b_1	1.89 ± 0.16
b_2	1.61 ± 0.13
c_1[a]	0.668 ± 0.389
c_2[a]	0.081 ± 0.013
Standard error	0.57
(b) Field – based weighting factors	
b_1	0.95 ± 0.14
b_2	1.35 ± 0.12
c_1	0.93 ± 0.49
c_2	0.123 ± 0.016
Standard error	0.53
(c) Averaged weighting factors	
b_1	1.53 ± 0.15
b_2	1.51 ± 0.12
c_1	0.75 ± 0.42
c_2	0.095 ± 0.014
Standard error	0.56

Liu et al. (2001) was considered as a major improvement in this field at that time considering that i) a significantly larger database was used, ii) this data was assessed probabilistically, and iii) different weighting factors were taken into account and their influence on the N – M_w correlations were presented.

More recently, Cetin and Bilge (2012) re-visited these concepts while developing their performance based magnitude duration factors. Their most interesting conclusion was

about the dependency of the "weighting factor" to the selected performance (failure) criterion and site conditions (Figure 2.4). In conjunction with the findings of Liu et al. (2001), Cetin and Bilge (2012) developed semi-empirical correlations for calculation of the weighting factor as a function of selected performance criterion (either in terms of cyclic shear strain or excess pore water pressure ratio), vertical effective stress and the relative density of the soil deposit.

On a separate stream of research, Green and Terri (2005) also focused on this issue by slightly modifying the Palmgren – Miner (P-M) cumulative damage hypothesis based on the dissipated energy during cyclic loading. The authors conducted a parametric study to develop correlations as a function of magnitude, site to source distance and depth in a soil profile of interest.

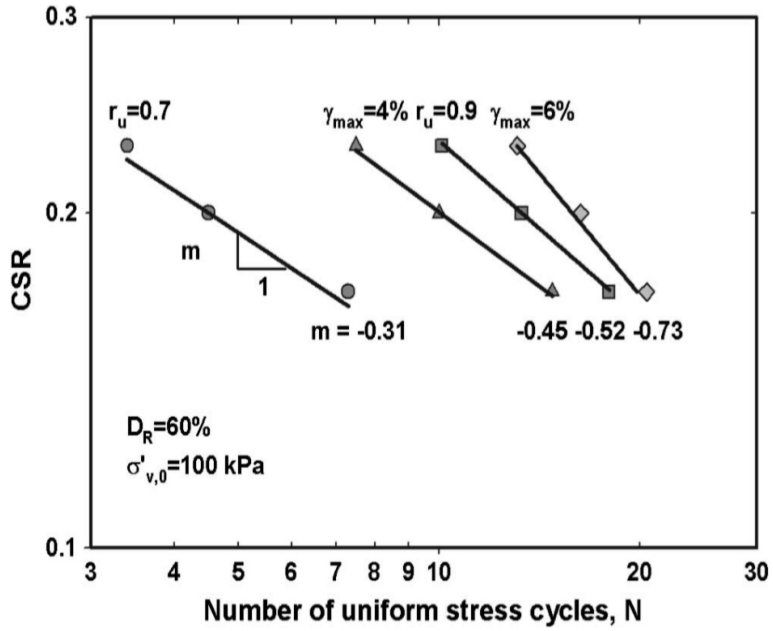

Figure 2.4. Variation of m with different performance criterions (after Cetin and Bilge 2012)

CHAPTER 3

DATABASE COMPILATION

3.1. Introduction

The database of this study includes 4176 records from 150 earthquakes by studying the Pacific Earthquake Engineering Research Center's ground motion database(www.peer.berkeley.edu). The resulting database includes data from 1935 Helena, Montana Earthquake to 2002 Denali, Alaska Earthquake. Magnitude (M_w) of these events, representative shear wave velocities of the top 30 m ($V_{s,30}$) of the corresponding measurement stations and Joyner-Boore distances (R_{jb}) vary in the ranges of 5.0 to 7.9, 116.35 m/s to 2016.13 m/s and 0 km to 365.14 km, respectively. Complete documentation of the database is available in Appendix A.

3.2. Database Distribution

As presented in Figure 3.1, the database includes earthquakes with magnitudes ranging from 5 to 7.9. In this context, there are a total of 42 earthquakes with magnitudes ranging from 5 to 5.5, 47 earthquakes with magnitudes ranging from 5.5 to 6, 22 earthquakes with magnitudes ranging from 6 to 6.5, 24 earthquakes with magnitudes ranging from 6.5 to 7, 11 earthquakes with magnitudes ranging from 7 to 7.5 and 4 earthquakes with magnitudes ranging from 7.5 to 8. The number of earthquakes with a magnitude between 5 and 6 constitutes approximately 59% of the database. On the other hand, earthquakes with magnitudes ranging from 7 to 8 constitutes only 10% of the database.

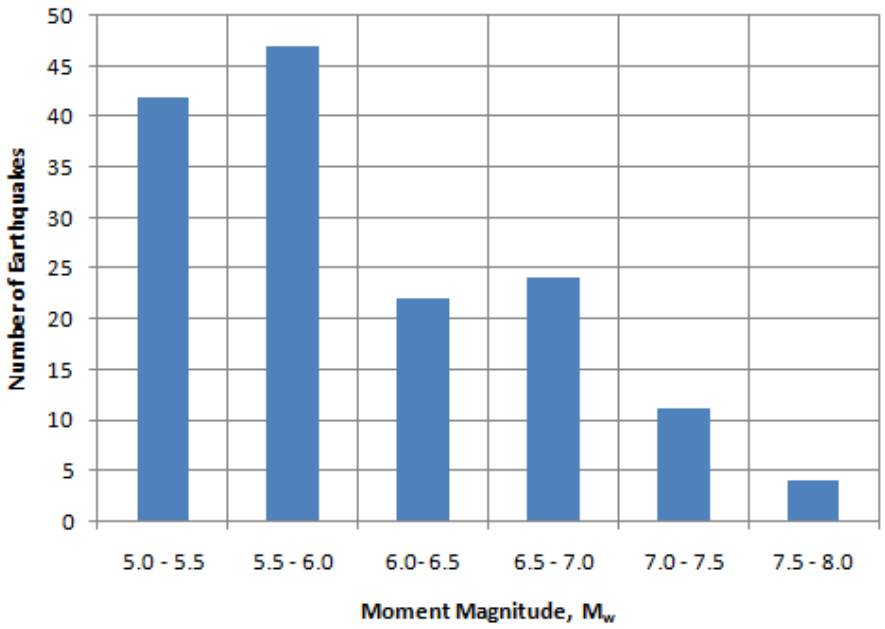

*Figure 3.1.*Number of earthquakes for different magnitude intervals

Figure 3.2 is prepared to present the variation of Joyner-Boore distance (R_{jb}) with moment magnitude. Boore and Atkinson (2008) stated that Joyner-Boore distance is approximately equal to epicentral distance for earthquake with $M_w < 6$. Therefore, for the records whose Joyner-Boore distance cannot be found and whose magnitude less than 6, epicentral distance was taken as Joyner-Boore distance. In general, R_{jb} values vary in the range of 0 km to 366 km. For earthquakes with magnitudes in the range of 5 to 6.5, R_{jb} mainly varies between 0 and 256 km. On the other hand, for earthquakes with magnitudes between 6.5 and 8, R_{jb} varies between 0 and 366 km.

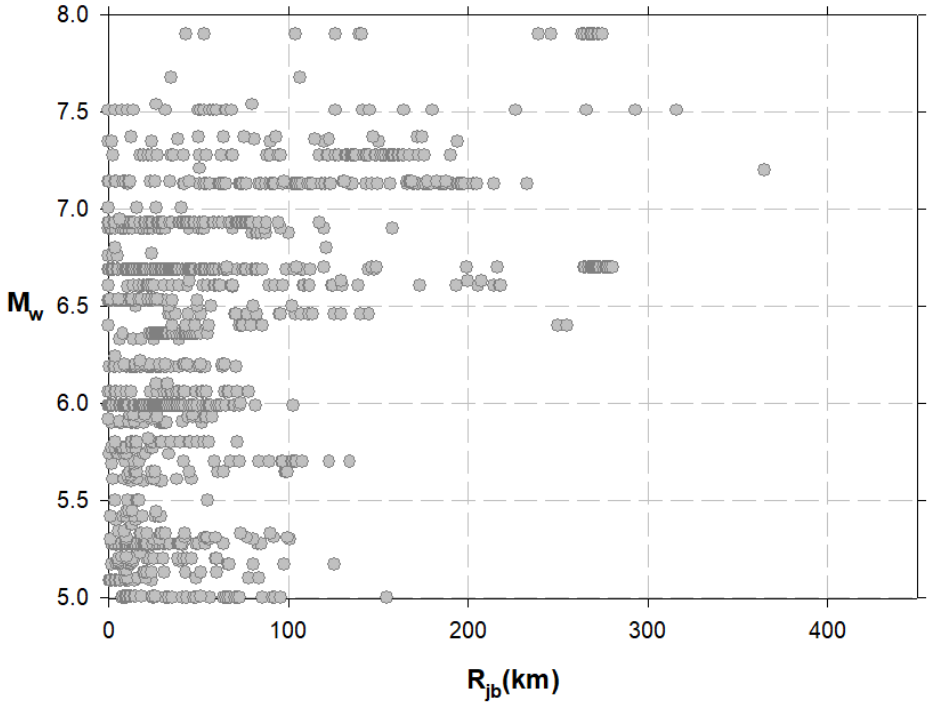

Figure 3.2. Distribution of magnitude and Joyner-Boore distance

Figure 3.3 presents the representative shear wave velocities of top 30 m ($V_{s,30}$) of the recording stations. For the compiled data, $V_{s,30}$ varies in the range of 116.35 m/s to 2016.13 m/s. For earthquakes having magnitude 5 to 7, $V_{s,30}$ mainly varies between 116.35 m/s and 2016.13 m/s. On the other hand, for earthquakes having magnitude 7 to 8, $V_{s,30}$ varies between 175 m/s and 963.94 m/s. As can be observed from Figure 3.3, $V_{s,30}$ of the data points are mainly in the range of 125 m/s to 750 m/s.

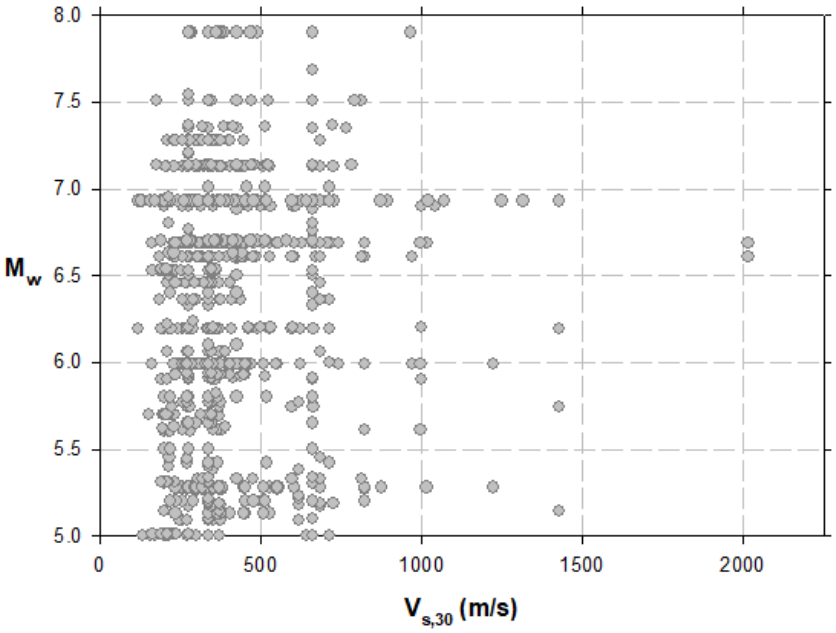

Figure 3.3. Distribution of magnitude and shear wave velocity

In conjunction with these shear wave velocity values, sites can also be classified by Geomatrix site type scheme (Table 3.1) as rock, stiff (shallow) soil, deep soil or soft soil. In case the site type is selected as A or B, then site is classified as "rock"; whereas, if the site type is C, D or E then it is classified as "soil". The compiled database is evaluated according to Table 3.1, and it is concluded that many of the measurement stations are located on soil sites.

Table 3.1. *Site type scheme*

Site Type	Classification
A	Rock (V_s>600 m/s) or less than 5 m soil above rock
B	Stiff (Shallow) Soil Thickness of 5 – 20 m soil above rock
C	In narrow canyon, deep soil Soil with a thickness of >20 m in a less than 2 km wide (narrow) canyon
D	In broad canyon, deep soil Soil with a thickness of >20 m in a larger than 2 km wide (broad) canyon
E	Soft Soil V_s< 150m/s

The distribution between shear wave velocity and Joyner-Boore distance is shown in Figure 3.4. For data having R_{jb} values varying between 0 and 100 km, $V_{s,30}$ mainly varies between 116.35 m/s – 1000 m/s.

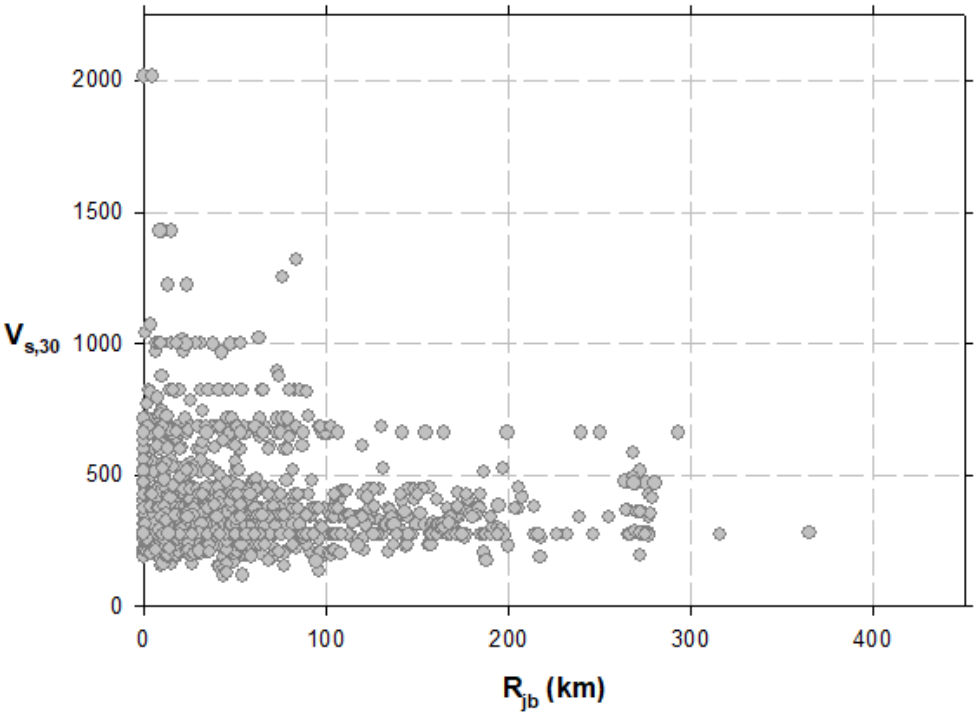

Figure 3.4. Distribution of shear wave velocity and Joyner-Boore distance

In order to follow the range of all parameters of the database, the 3D graph showing the distribution between M_w, $V_{s,30}$ and R_{jb} values is presented in Figure 3.5.

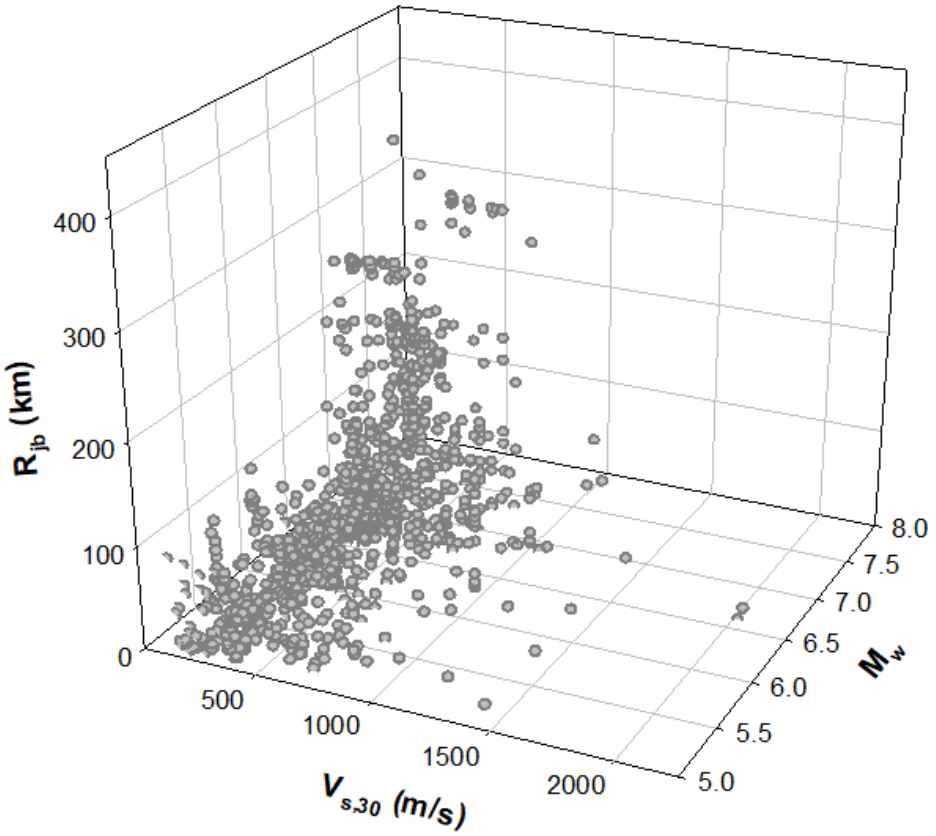

Figure 3.5. Distribution of magnitude, shear wave velocity and Joyner-Boore distance

Strong motion data were obtained from the web site of the Pacific Earthquake Engineering Research Center (www.peer.berkeley.edu). Inspection of acceleration time history data reveals that time interval of the records is not constant. In order to eliminate the influence of this variation, all data were decimated to a common time step of 0.02 seconds by first applying a low-pass filter having a corner frequency of 25 Hz (4^{th} order Chebyshev) and then re-sampling it with time step of 0.02 seconds.

All irregular acceleration time histories were then converted to equivalent uniform stress cycles by following the procedure given by Seed et al. (1975). As stated in Chapter 2, this approach involves a weighting factor, which is now known to be a function of selected performance criterion along with site conditions (vertical effective stress and relative density) (Cetin and Bilge, 2012). In order to take into account, the effect of weighting factor, equivalent uniform stress cycles were counted for each

acceleration time histories for 17 different weighting factors; 0.2, 0.25, 0.3, 0.37, 0.41, 0.45,0.5, 0.55, 0.6, 0.65,0.7,0.75, 0.8, 0.85, 0.9, 0.95 and 1.0 (0.37, 0.41 and 0.5 were selected for further comparison with the model of Liu et al. 2001). At the end of counting, 70483 data points were collected.

Distributions between counted number of cycles (N) and moment magnitude (M_w), shear wave velocity ($V_{s,30}$) and Joyner-Boore distance (R_{jb}) are presented in Figure 3.4, Figure 3.5 and Figure 3.6, respectively. The existing trends of the database will be discussed in Chapter 4.

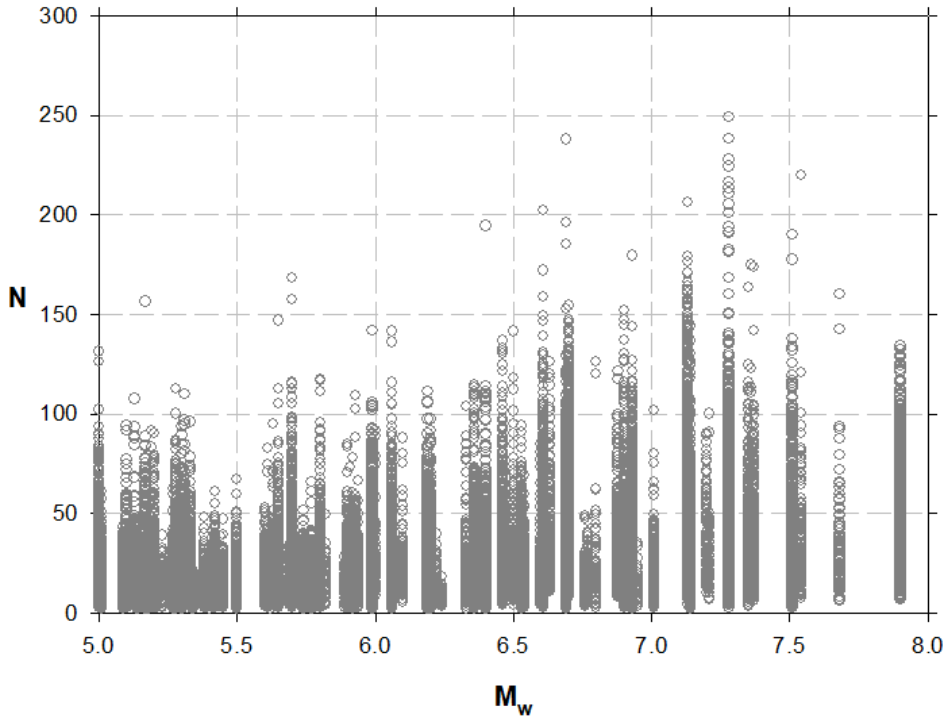

Figure 3.6. Distribution of N with M_w

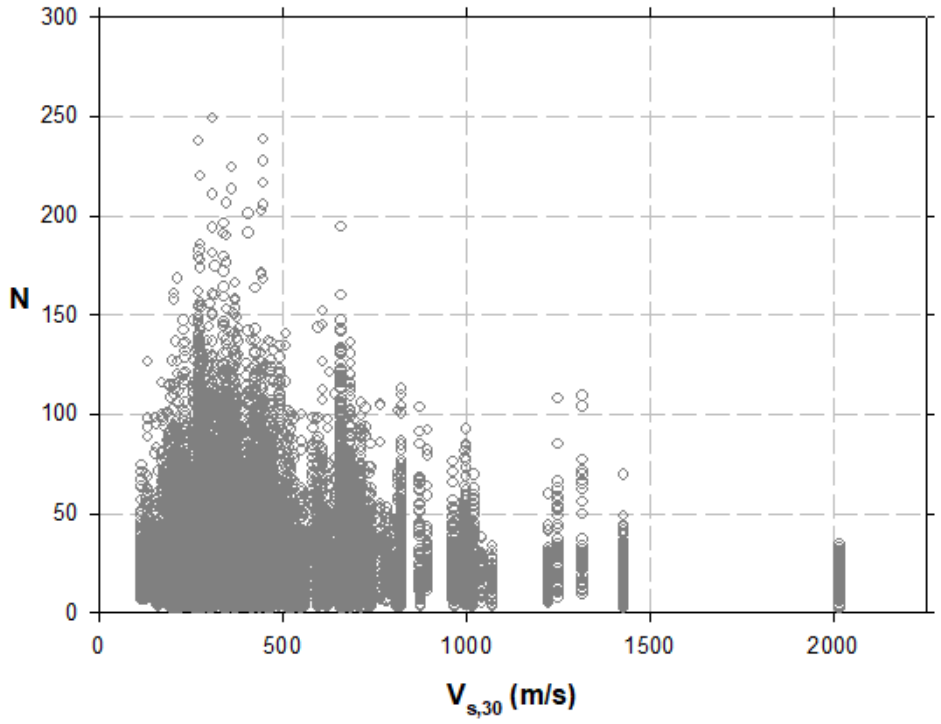

Figure 3.7. Distribution of N with $V_{s,30}$

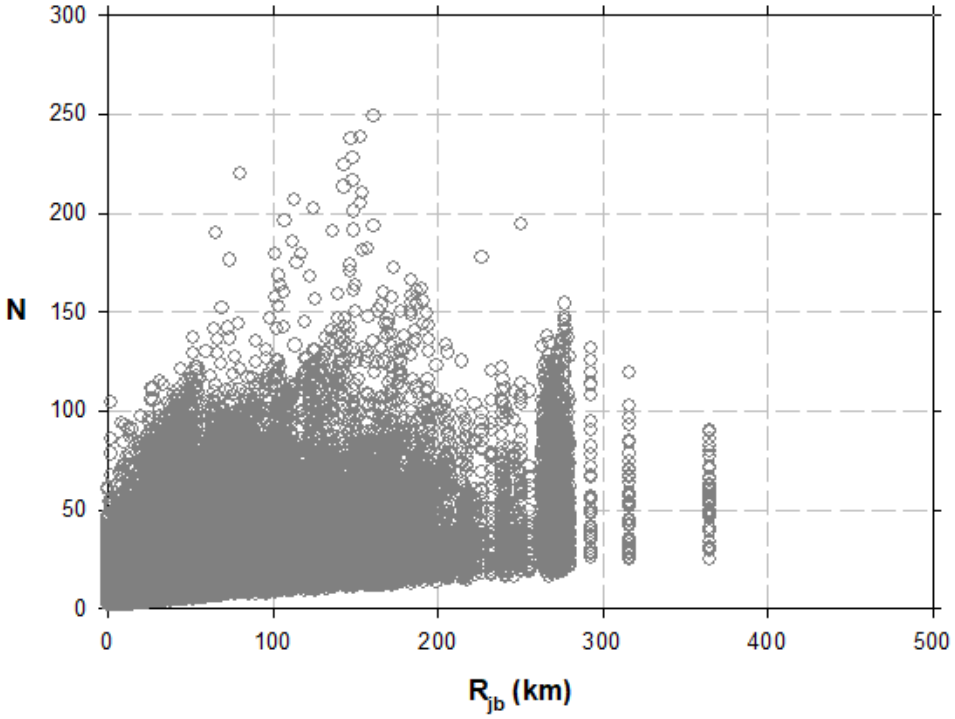

Figure 3.8. Distribution of N with R_{jb}

CHAPTER 4

INTERPRETATION OF DATABASE TRENDS AND DEVELOPMENT OF PROBABILISTIC MODELS

4.1. Introduction

Within the confines of this chapter, first the existing trends of the database will be discussed in terms of number of equivalent uniform stress cycles and moment magnitude, site - source distance and site characteristics. For this purpose, comparison graphs including number of equivalent uniform stress cycles vs. moment magnitude (M_w), representative shear wave velocity of the measurement station ($V_{s,30}$), Joyner-Boore distance (R_{jb}) and weighting factor (m) are plotted for the purpose of investigating the possible relationships between N - M_w, N - $V_{s,30}$, N –R_{jb} and N - m. Then based on these plots, probabilistic models capturing the relationship between N - M_w, $V_{s,30}$, R_{jb} and m are developed in the second part of this chapter.

4.2. Assessment of Database Trends

For the sake of completeness, relationships between counted number of cycles, N values and moment magnitude, M_w, shear wave velocity, $V_{s,30}$ and Joyner-Boore distance, R_{jb} are presented again in Figure 4.1, Figure 4.2 and Figure 4.3, respectively.

As shown in Figure 4.1, number of uniform stress cycles is increasing with moment magnitude of earthquake. In more detail, the number of equivalent uniform cycle increases approximately twice as the moment magnitude increases.

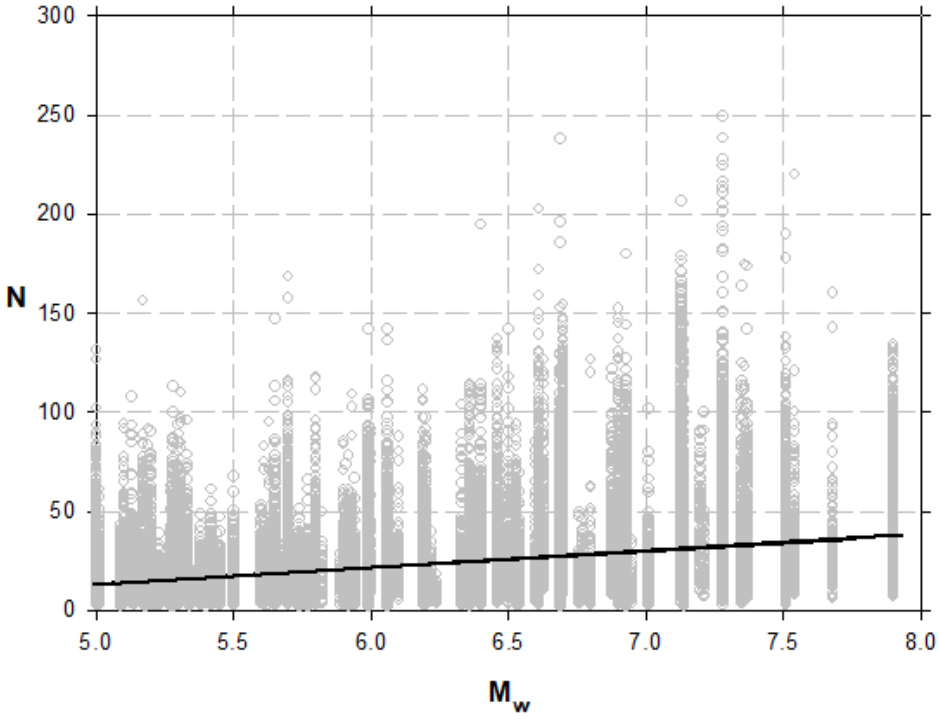

Figure 4.1. Distribution of N with M_w

As presented in Figure 4.2, number of uniform stress cycles is decreasing while shear wave velocity is increasing. More specifically, number of equivalent uniform stress cycle decreases dramatically, particularly if the shear wave velocity is greater than 500 m/s.

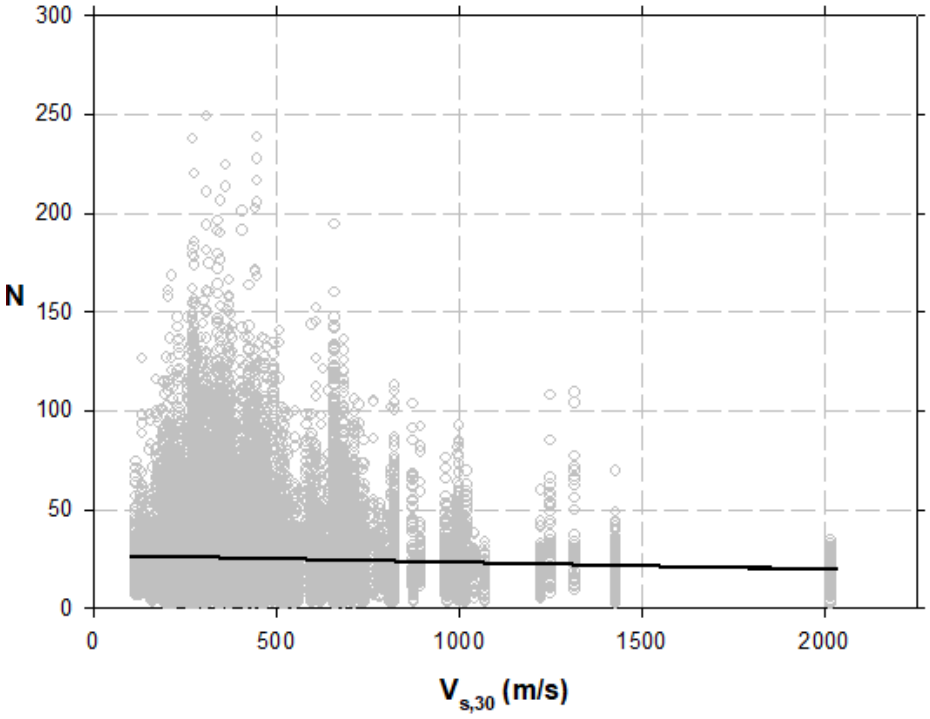

Figure 4.2. Distribution of N with $V_{s,30}$

Similar to moment magnitude and shear wave velocity trends, number of uniform stress cycle is increasing with Joyner-Boore distance. In more detail, the tendency of number of equivalent uniform stress cycles to increase with Joyner-Boore distance higher, when the Joyner-Boore distance is between 0 and 200 km.

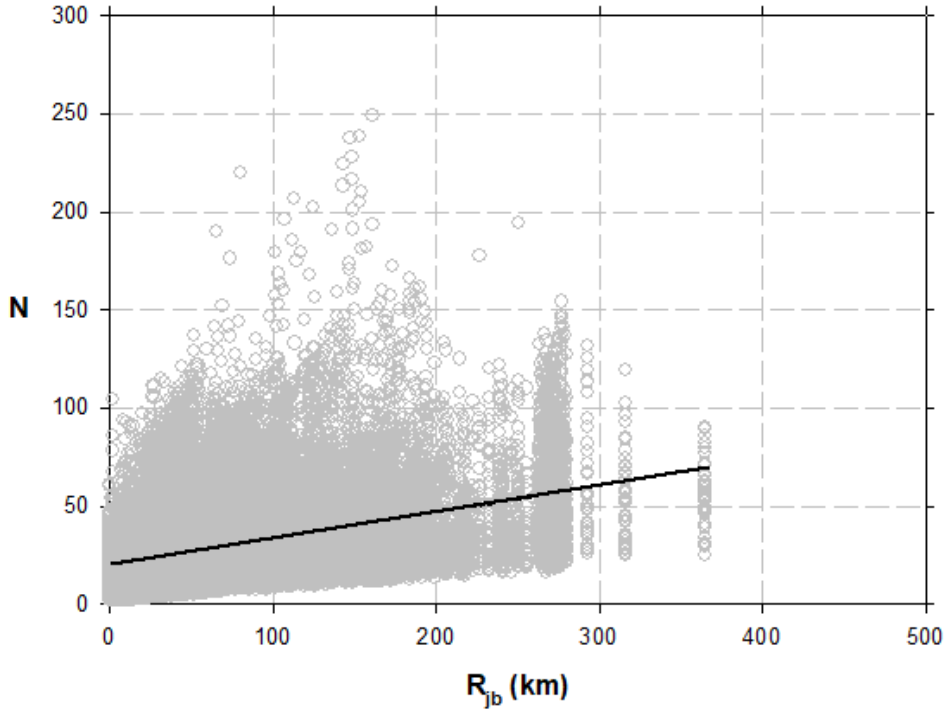

Figure 4.3. Distribution of N with R_{jb}

Aside from M_w, $V_{s,30}$ and R_{jb}, counted number of equivalent uniform stress cycle varies also with the selected weighting factor. Relationship between average number of cycle (for data presentation purposes, magnitude bins are defined and the average values are calculated for each bin separately) and weighting factor (m) is presented in Figure 4.4. As shown in Figure 4.4, number of cycles decrease up to some point (this point varies as a function of M_w but it is in the order of 0.25 - 0.30) but after this point N values tend to increase as the weighting factor increases. In addition, Figure 4.4 also reveals that number of cycle with moment magnitude of earthquake similar with presented trend presented in Figure 4.1 and its related discussion.

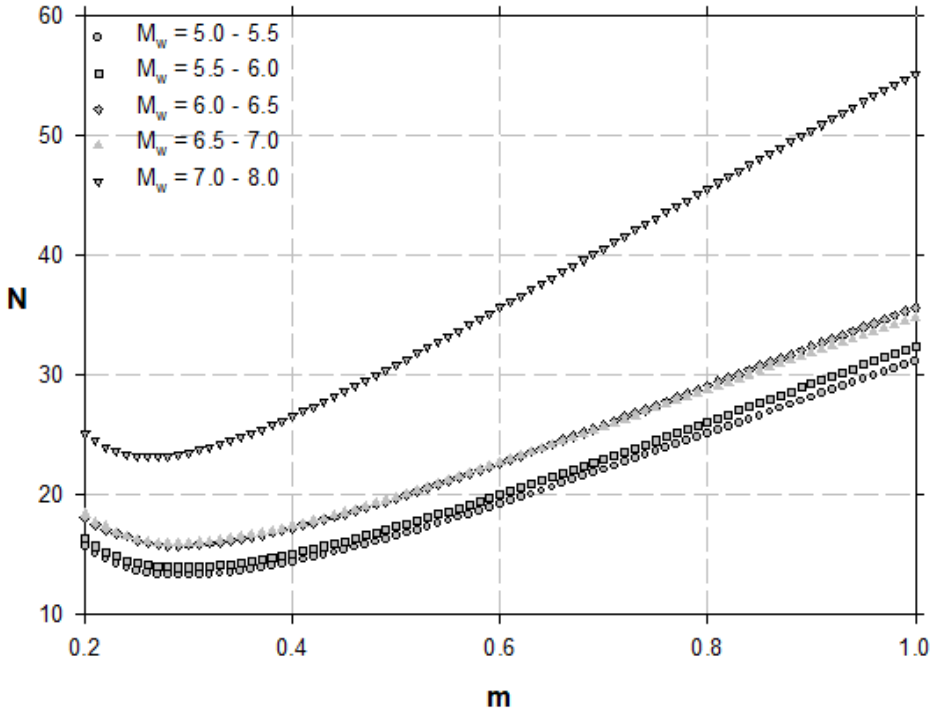

Figure 4.4. Relationship between number of cycle and weighting factor for different moment magnitude ranges

4.2.1. Unified Field Classification Based On M_w, R_{jb} and $V_{s,30}$

Discussion presented in Section 4.1 has clearly revealed the dependency of number of equivalent stress cycles to moment magnitude, Joyner-Boore distance and representative shear wave velocity of the measurement station. However, considering the quite wide ranges of M_w, R_{jb} and $V_{s,30}$ values, it is realized that the existing trends cannot be accurately quantified in case the whole database is assessed at once. In order to provide a basis for more accurate assessment, different bins of M_w, R_{jb} and $V_{s,30}$ are defined. For this purpose, representative M_w values are selected as 5.0, 5.5, 6.0, 6.5, 7.0, 7.5 and 8.0; whereas $V_{s,30}$ bins are defined to represent soft soil sites ($V_{s,30}$ = 75 m/s), relatively medium stiff soil sites ($V_{s,30}$ = 225 m/s) and hard sites ($V_{s,30}$ = 500 m/s). On the other hand, preliminary inspection on existing data reveals that the effect of site – source distance on N cannot be explained adequately by using Joyner-Boore distance as the sole parameter. It is realized that site – source distance effects vary as a function of M_w and $V_{s,30}$ as well (i.e. definition of near-, mid- and far-field site

definitions). Consequently, it is decided to benefit from the existing ground motion prediction equations (GMPE) to define these site – source distance bins more properly. Within the confines of this study, it is decided to use the relations provided by Boore and Atkinson (2008) which was presented as part of NGA (2008). This method is selected since it is one of the most widely referred studies in this field and also it is easy to use. Details of Boore and Atkinson (2008) ground motion prediction model will not be presented herein; however, the median peak ground acceleration (PGA) predictions of this method for the $V_{s,30}$ bins of 75 m/s, 225 m/s and 500 m/s are presented in Figures 4.5, 4.6 and 4.7, respectively.

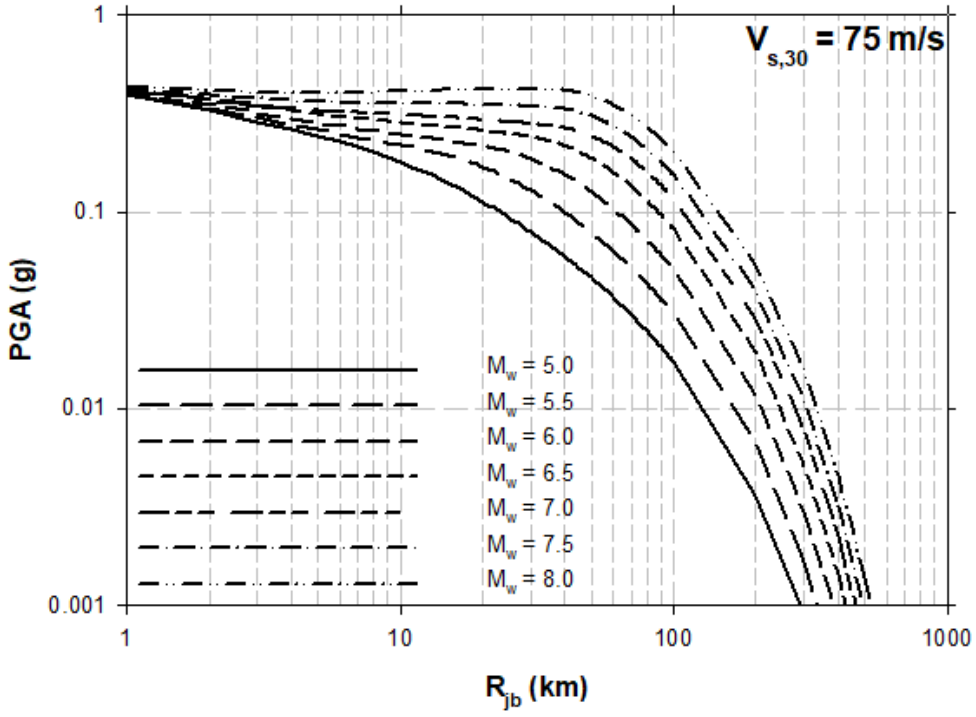

Figure 4.5. GMPE predictions for $V_{s,30}$ = 75 m/s

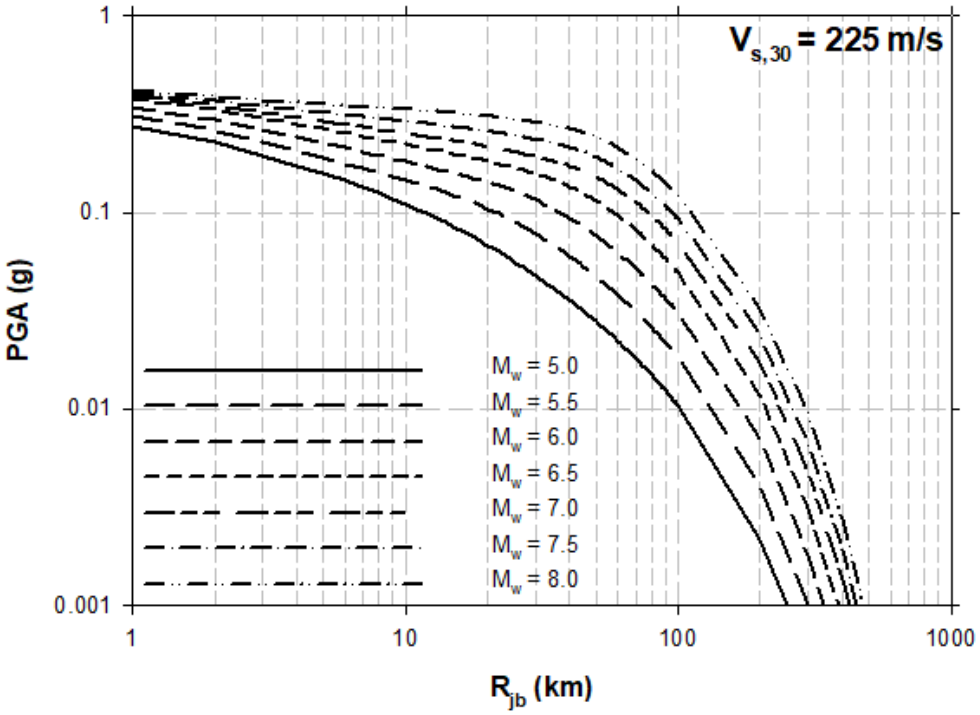

Figure 4.6. GMPE predictions for $V_{s,30}$ = 225 m/s

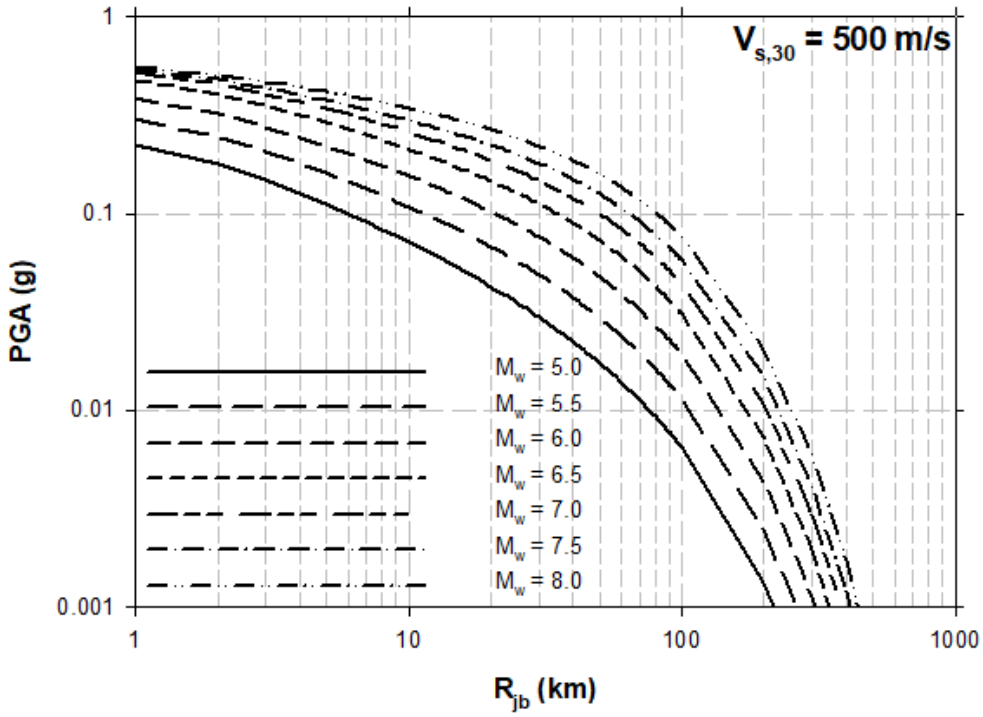

Figure 4.7. GMPE predictions for $V_{s,30}$ = 500 m/s

As presented in Figures 4.5, 4.6 and 4.7, these plots consist of 2 linear and 1 non-linear regions. Consistent with the existing terminology, the 1st region, where the curve is linear, is used to define the near-field sites, the 2nd region, where the curve is non-linear, is used to define the mid-field sites and the 3rd region, where the curve is linear again, is used to define far-field sites. As highlighted by these figures, these site distance definitions vary as a function of both $V_{s,30}$ and M_w. Figure 4.8 presents how these field definitions are made for relatively stiffer soil sites ($V_{s,30}$ = 225 m/s) and M_w =8.0 earthquake.

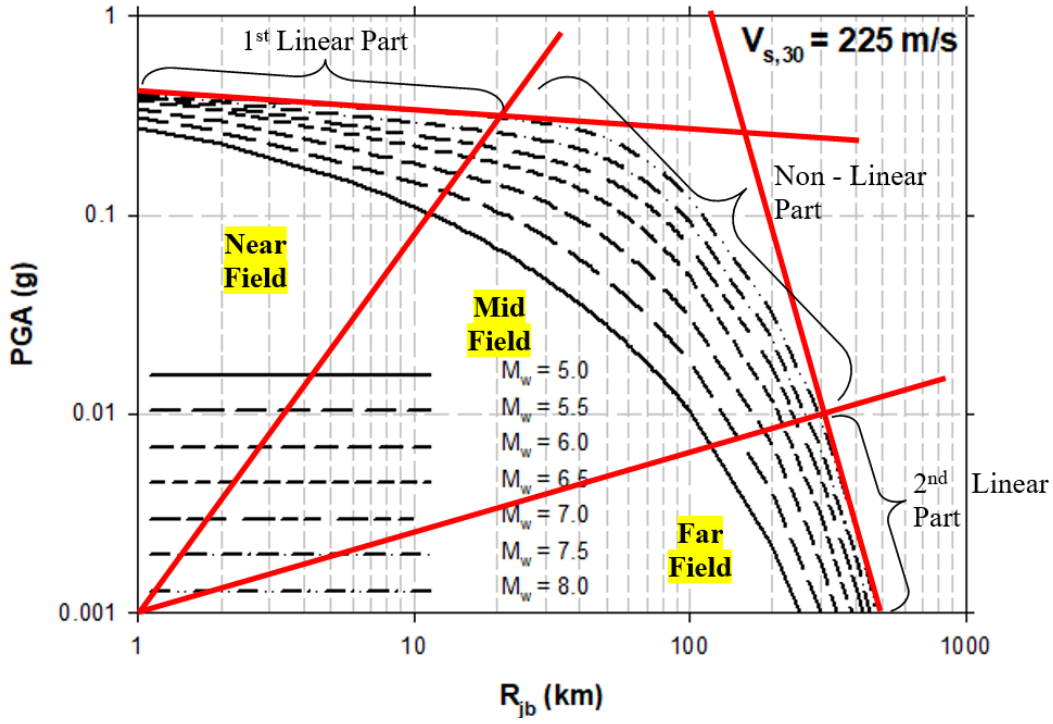

Figure 4.8. Site – source distance definitions according for $V_{s,30}$=225 m/s and M_w=8.0 case

As schematically presented in Figure 4.8, the near-field boundary (r_{near}) was determined as a distance term, where the 1st linear portion was approximately terminated for a given shear wave velocity and the moment magnitude. Similar to the near-field limit, the far-field boundary (r_{far}) was also determined as the distance term, where 2nd linear portion starts. In this case, the area between the near-field and the far-field boundaries was defined as mid-field. Selected limits for the near- and far-fields

for each M_w and $V_{s,30}$ based on the ground motion prediction method of Boore and Atkinson (2008) are summarized in Table 4.1.

Table 4.1. *Determined near field and far field limits*

Moment Magnitude, M_w	Near Field Limit, r_{near} (km)	Far Field Limit, r_{far} (km)
Shear Wave Velocity, $V_{s,30}$ = 75 m/s		
5.0	6	200
5.5	15	225
6.0	16	250
6.5	18	300
7.0	20	350
7.5	30	375
8.0	40	400
Shear Wave Velocity, $V_{s,30}$ = 225 m/s		
5.0	2	200
5.5	2.5	220
6.0	3	240
6.5	4	275
7.0	15	280
7.5	18	300
8.0	20	315
Shear Wave Velocity, $V_{s,30}$ = 500 m/s		
5.0	1.5	200
5.5	1.7	220
6.0	1.8	235
6.5	2	250
7.0	2.5	260
7.5	3	275
8.0	6	300

Data presented in Table 4.1 which define near- and far-field boundaries as a function of M_w are schematically presented in Figures 4.9 and 4.10, respectively for the selected $V_{s,30}$ values of 75 m/s, 225 m/s $V_{s,30}$ = 500 m/s.

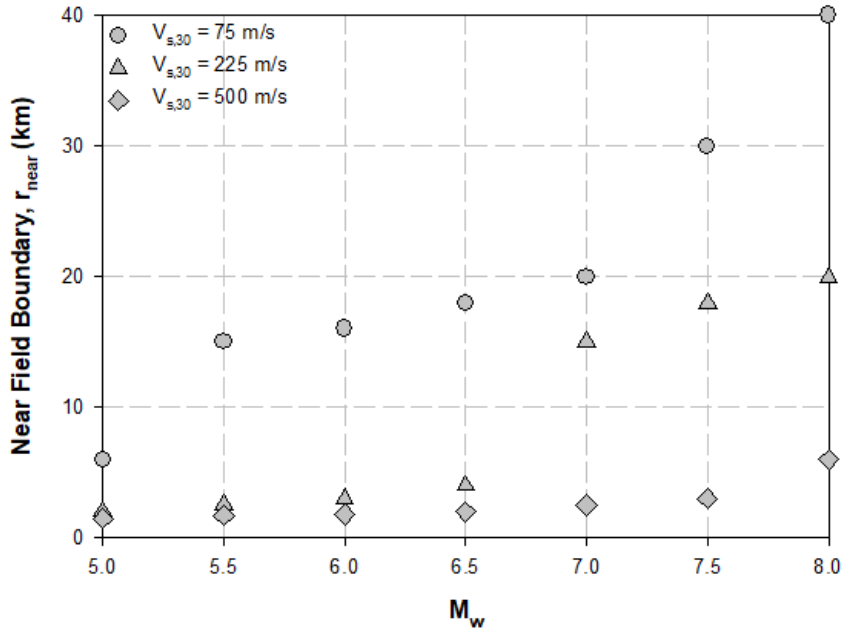

Figure 4.9. Near-field site limits vs. moment magnitude relationship

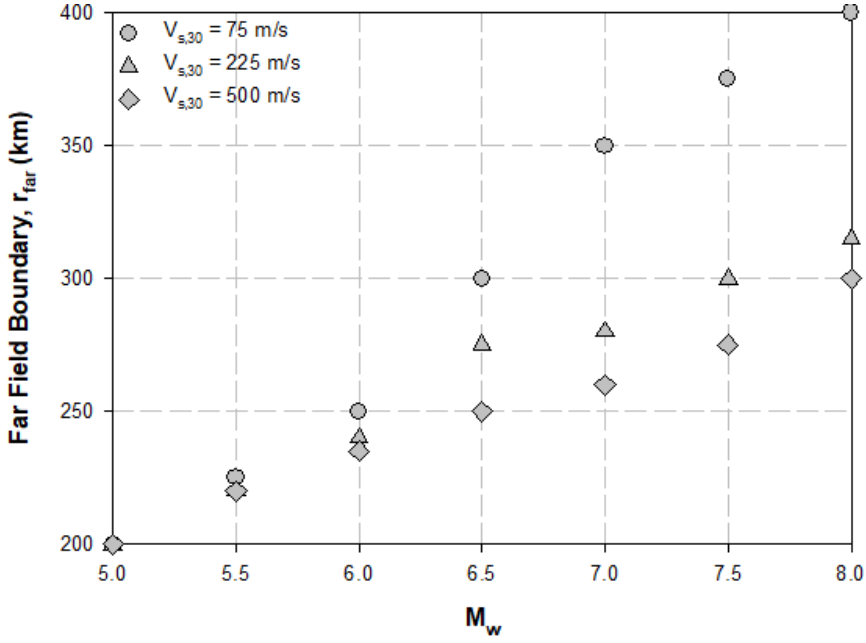

Figure 4.10. Far-field site limits vs. moment magnitude relationship

The relations presented in Figure 4.9 and 4.10 are quantified by following a regression analysis, and r_{near} and r_{far} terms are expressed as functions of $V_{s,30}$ and M_w as presented in Equation 4.1 and 4.2, respectively.

$$r_{near} = 0.5 * e^{\frac{2.37*M_w}{\ln(V_{s,30})}} \quad (4.1)$$

$$r_{far} = 85 * e^{\frac{0.4*M_w}{\sqrt{\ln(V_{s,30})}}} \quad (4.2)$$

where M_w and $V_{s,30}$ denote moment magnitude and average shear wave velocity in the top 30 m, respectively. In summary, if the distance term (R_{jb}) of a specified case is lower than the calculated r_{near} value (for case's corresponding M_w and $V_{s,30}$), then the record is classified as a near-field record. If the distance term (R_{jb}) is greater than calculated r_{far}, then the record is classified as a far-field record. In case, the distance term (R_{jb}) falls in between r_{near} and r_{far}, then it is classified as a mid-field record. The sensitivity of the r_{near} and r_{far} model coefficients on the overall model accuracy and sensitivity is tested through maximum likelihood assessments by using different r_{near} and r_{far} model coefficients. Owing to minor changes in the maximum likelihood values, it is concluded that r_{near} and r_{far} model coefficients (i.e.: 0.5, 2.37, 85, 0.4) given in Equations 4.1 and 4.2 are not significant from overall model performance point of view. The discussion of model performances will be presented in Chapter 5. However, for the sake of simplicity, these sensitivity analyses and their results will not be presented herein.

4.2.2. Database Trends for Different Unified Field Classes

This section is devoted to the interpretation of database trends for near-, mid- and far-field record classes according to the definitions introduced in Section 4.1.1.

For the near-field records, variation of counted number of equivalent uniform cycles as a function of M_w, $V_{s,30}$ and R_{jb} are presented in Figure 4.11, Figure 4.12 and Figure 4.13, respectively. The data exhibits similar trends with those presented in Figures 4.1 and 4.3. N exhibits a slightly increasing overall trend with increasing M_w or R_{jb}; on

the other side, N values slightly increase for increasing $V_{s,30}$ values at sites classified as near-field. Trend lines determined by linear regression are presented on these figures to support these conclusions. As it provides a better representation, the y-axis of these graphs are presented in ln-scale. This choice becomes more important for mid- and far-field sites as will be discussed next, but for the sake of consistency it is preferred to present all of these plots in a similar manner.

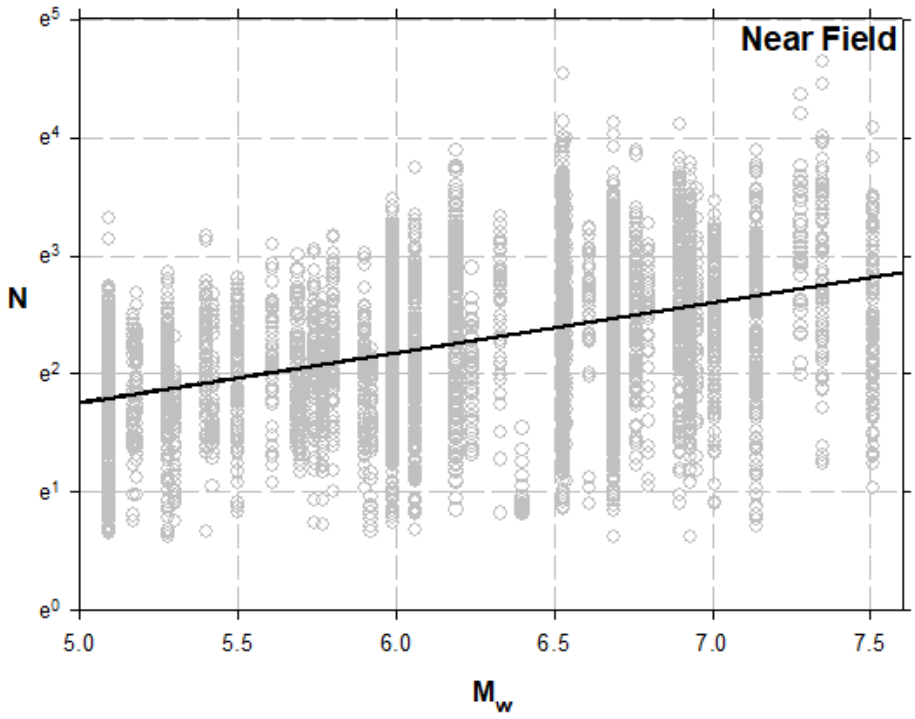

Figure 4.11. Distribution of N and M_w for near field cases

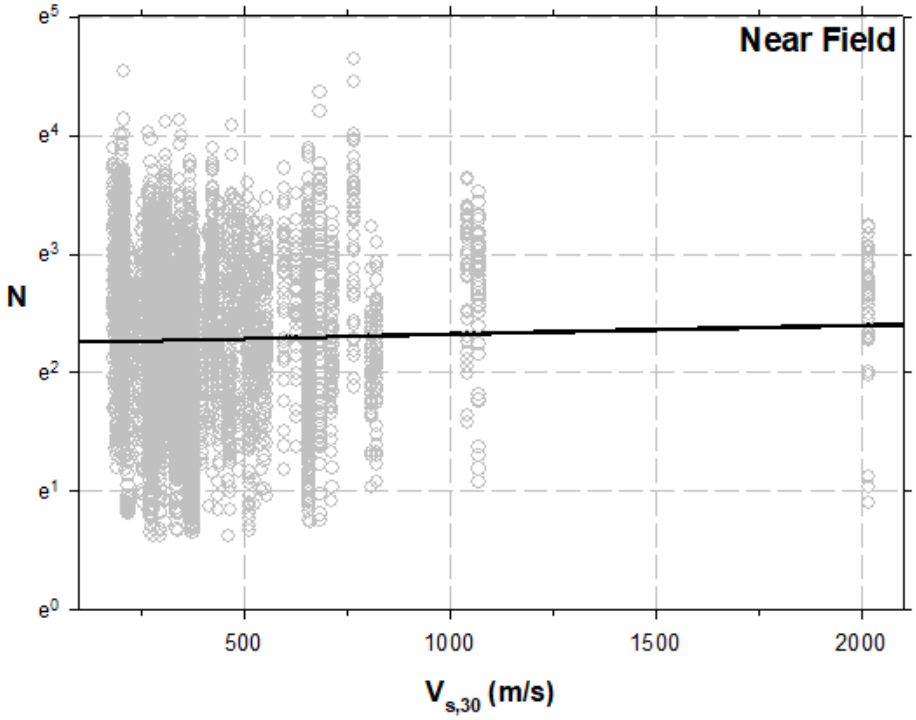

Figure 4.12. Distribution of N and $V_{s,30}$ for near field cases

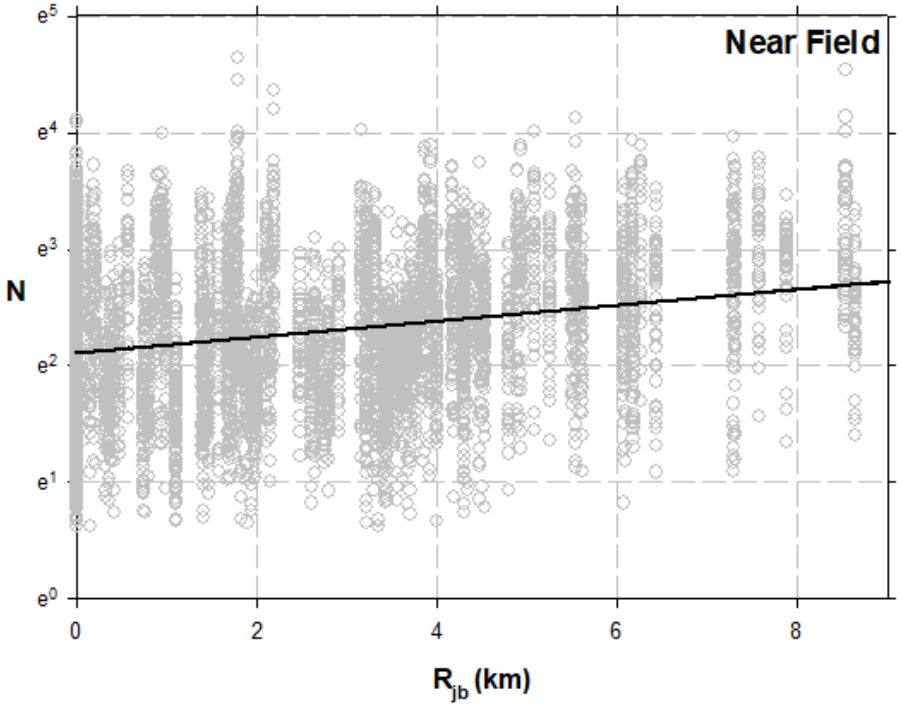

Figure 4.13. Distribution of N and R_{jb} for near field cases

For earthquake records classified as mid-field, the variation of counted number of equivalent uniform cycles as a function of M_w, $V_{s,30}$ and R_{jb} are presented in Figure 4.14, Figure 4.15 and Figure 4.16, respectively. The data exhibits similar trends with those presented in Figures 4.1, 4.2 and 4.3. N exhibits a slightly increasing overall trend with increasing M_w or R_{jb}; whereas, N values decrease for increasing $V_{s,30}$ values at sites classified as mid-field. Trend lines determined by linear regression are presented on these figures to support these conclusions. As it provides a better representation, the y-axis of these graphs are presented in log-scale. In addition, this classification effort has revealed that approximately 88% of the earthquakes can be classified as mid-field. Since most of the earthquakes in the database are classified as mid field, these data will have a large impact on the development of relationships.

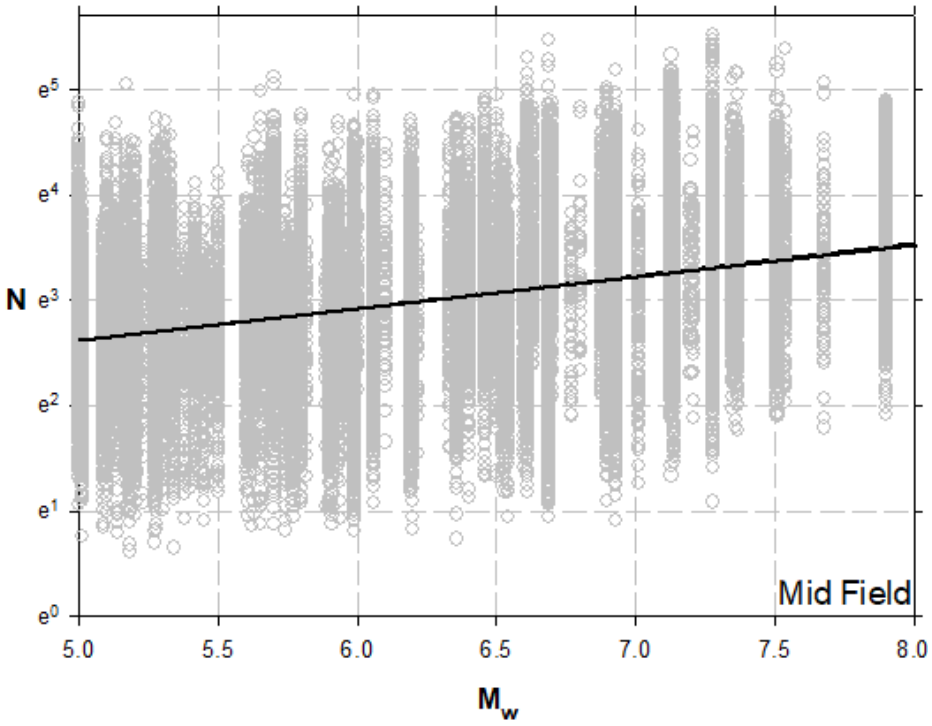

Figure 4.14. Distribution of N and M_w for mid field cases

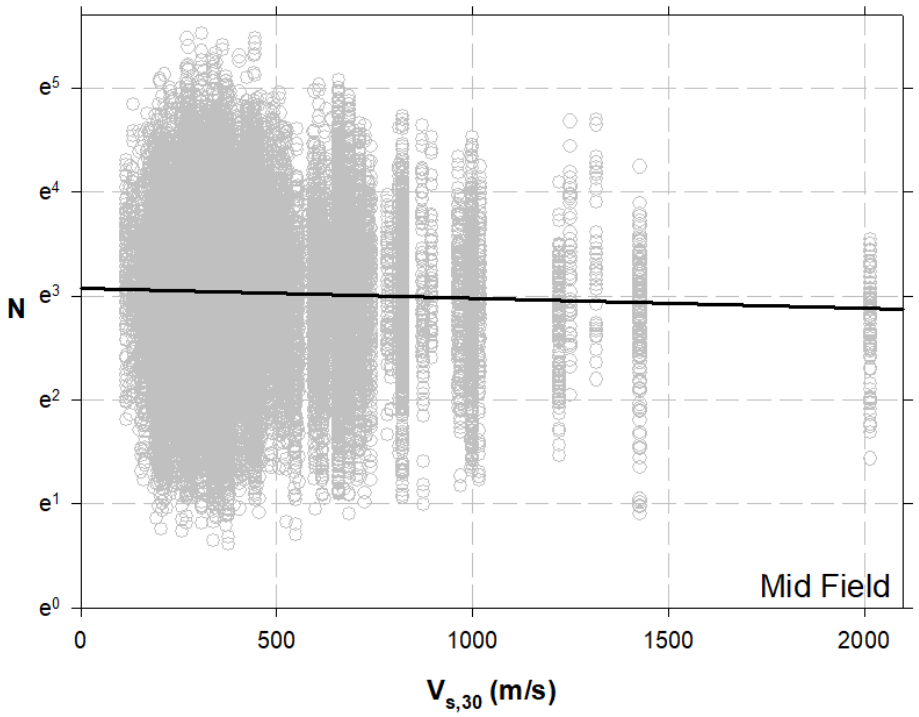

Figure 4.15. Distribution of N and $V_{s,30}$ for mid field cases

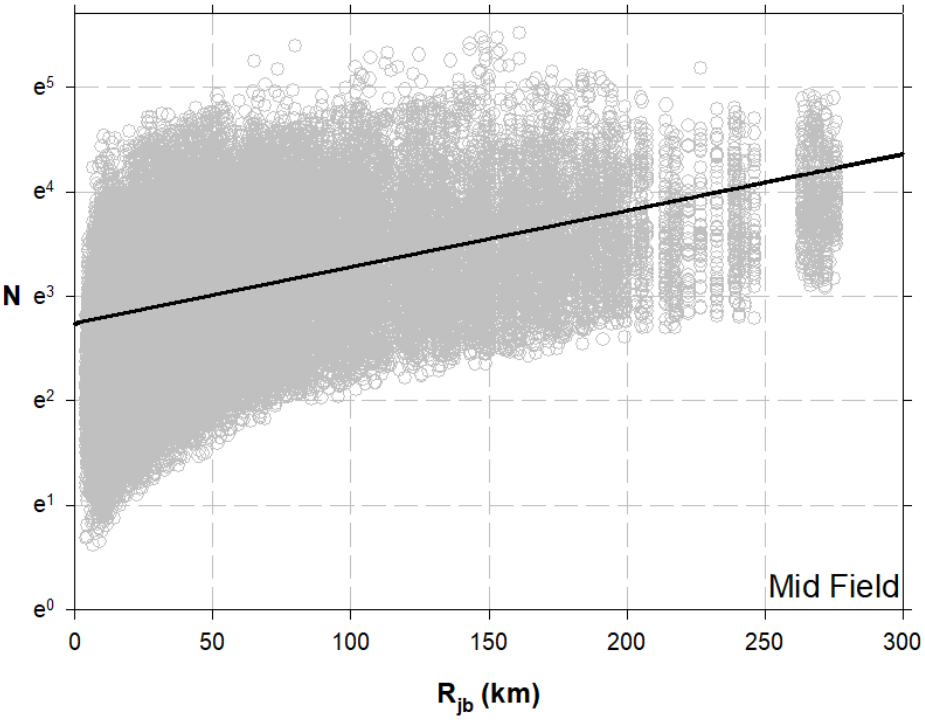

Figure 4.16. Distribution of N and R_{jb} for mid field cases

For the far-field records, distribution of counted number of equivalent uniform cycle and moment magnitude, shear wave velocity and Joyner-Boore distance are presented in Figure 4.17, Figure 4.18 and Figure 4.19, respectively. Similar to mid field earthquake records, the data exhibits similar trends with those presented in Figures 4.1, 4.2 and 4.3. N exhibits a slightly increasing overall trend with increasing M_w or r; whereas, N values decrease for increasing $V_{s,30}$ values at sites classified. Trend lines determined by linear regression are presented on these figures to support these conclusions. After all the cases of the database are classified, approximately 2.5% of the earthquakes are classified as far-field.

These trends will constitute the basis of the model development efforts which will be discussed next.

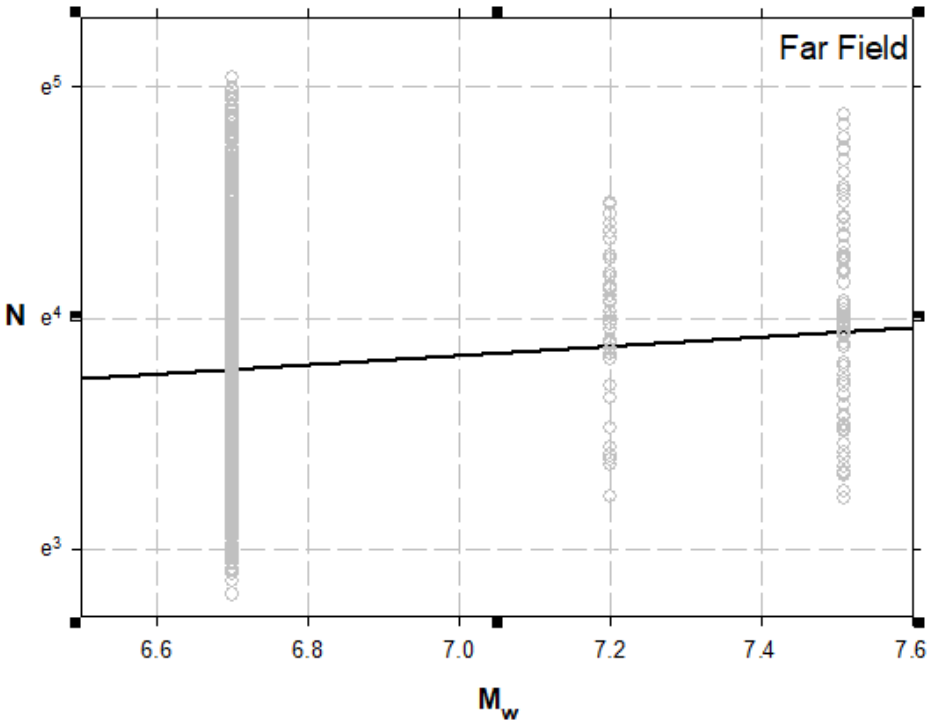

Figure 4.17. Distribution of N and M_w for far field cases

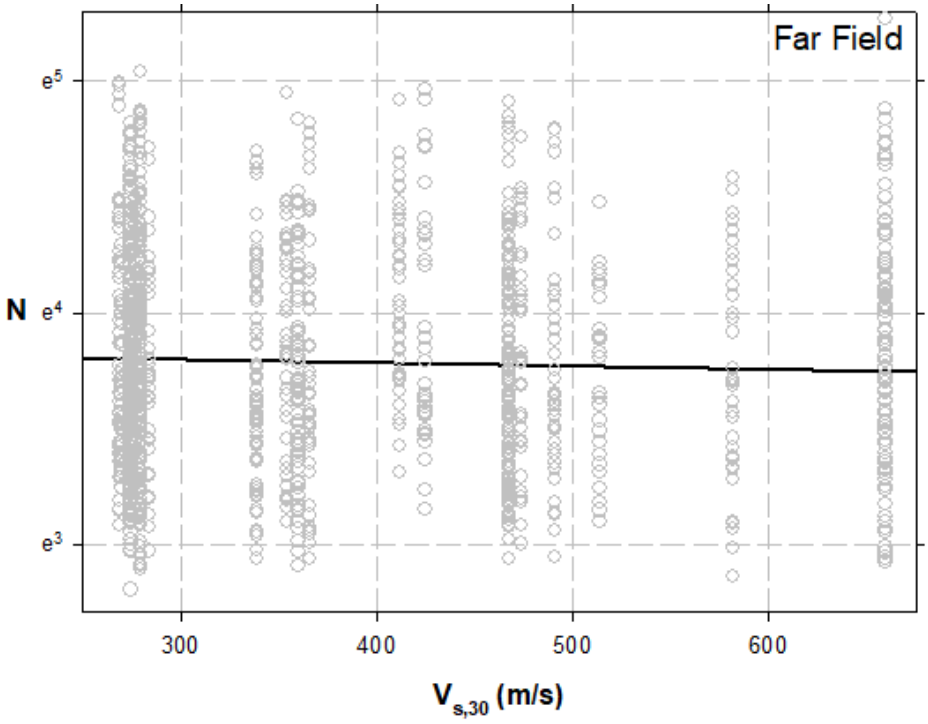

Figure 4.18. Distribution of N and $V_{s,30}$ for far field cases

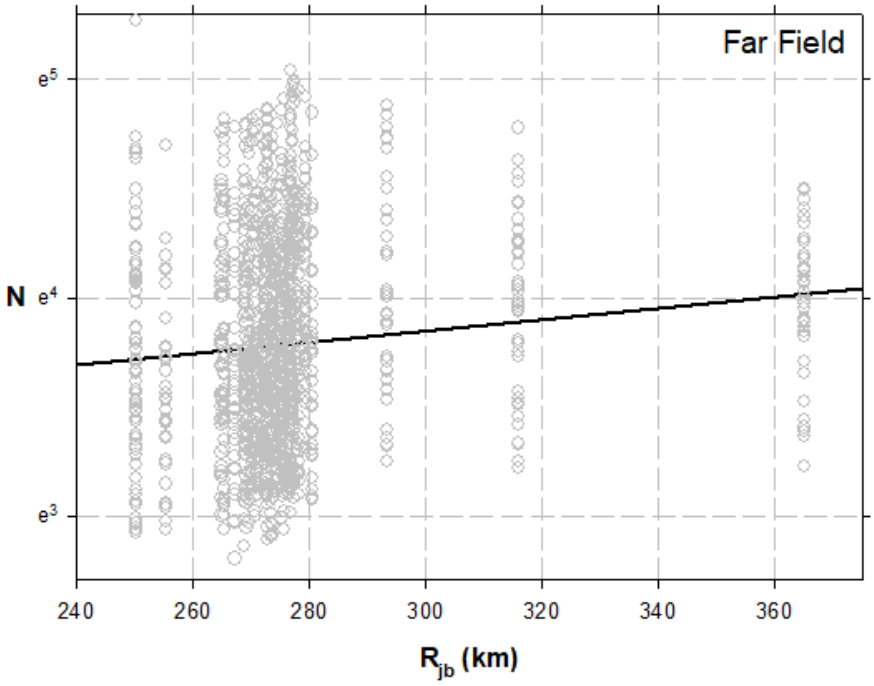

Figure 4.19. Distribution of N and R_{jb} for far field cases

4.3. Development of Semi – Empirical Models

Efforts aiming to develop a semi-empirical or an empirical model naturally require the compilation of a high quality database, which was introduced in Chapter 3. This data is critically reviewed as discussed in Section 4.1, and its interpretation will constitute the basis of the model development efforts which will be presented within the confines of this section.

As introduced as part of the literature survey, study of Liu et al. (2001) is considered as a main inspiration for this research. Yet, Liu et al. (2001) stated that only 1528 cases were used in model development stage. For this reason, the starting point is to evaluate the performance of Liu et al. model by using the compiled database in this research (closest distances to the rupture plane were also compiled, since it was used as site-source distance in Liu et. al (2001)), and then the model coefficients of Liu et al. model will be calibrated by using maximum likelihood methodology. After evaluating the performance of Liu et al. (2001), new models will be assessed by using the data analyzed in this study.

4.3.1. Performance Assessment of Liu et al. (2001) Model

Details of Liu et al. (2001) were presented in Chapter 2, yet the proposed expression is given in Equation 4.3 as a reminder; whereas, the model coefficients are summarized in Table 4.2

$$\ln(N) = ln\left[\frac{\left(\frac{\exp(b_1+b_2(m-m^*))}{10^{1.5m+16.05}}\right)^{-1/3}}{4.9*10^6\beta} + Sc_1 + rc_2\right] + \varepsilon \qquad (4.3)$$

Table 4.2. *Coefficients estimated by Liu (2001)*

Coefficients	Estimate
(a) Laboratory – based weighting factors	
b_1	1.89 ± 0.16
b_2	1.61 ± 0.13
c_1	0.668 ± 0.389
c_2	0.081 ± 0.013
Standard error	0.57
(b) Field – based weighting factors	
b_1	0.95 ± 0.14
b_2	1.35 ± 0.12
c_1	0.93 ± 0.49
c_2	0.123 ± 0.016
Standard error	0.53
(c) Averaged weighting factors	
b_1	1.53 ± 0.15
b_2	1.51 ± 0.12
c_1	0.75 ± 0.42
c_2	0.095 ± 0.014
Standard error	0.56

Liu et al. (2001) stated that the residuals were used to quantify the rupture directivity effects on number of cycles for near-source sites. It was also mentioned that for the cases with M_w>6.5 and r<20 km, mean residuals needed to be calculated and added to ln(N) calculated from Equation 4.3. In order to perform more fair performance analysis, the cases satisfying these conditions were excluded from the evaluations made in this section.

Liu et al. (2001) presented 3 different set of solutions for 3 different weighting factors (m = 0.37 (laboratory based), m=0.41 (average) and m= 0.5 (field based)). Therefore,

in performance assessment analyses, data corresponding to these weighting factors were taken into account. For these cases, residuals (defined as the difference of natural logarithm of the counted and predicted values) were calculated and presented as a function of the model parameters (moment magnitude, site - source distance and shear wave velocity) in Figures 4.20 through 4.28. The calculated mean and standard deviation of the residuals are also presented in these figures. As part of these plots the mean values of the residuals ($\mu_{residual}$) (by solid line) along with $\mu_{residual}\pm\sigma_{residual}$ (by medium dash line) and $\mu_{residual}\pm3\sigma_{residual}$ (by short dash line) are also presented to provide an insight on possible bias of the revised model.

Figures 4.20 to 4.22 present the assessments conducted for the laboratory based weighting factor (i.e. m = 0.37). The residual plots along with their statistical descriptors reveal that the predictions of Liu et al. (2001) model is producing estimates that are lower than number of cycle values determined by Seed et al. (1975) method. In the average, the difference is in the order of 4.4%.

Figures 4.23 to 4.25 present the assessments conducted for the weighting factors corresponding to average case (i.e. m = 0.41). The residual plots along with their statistical descriptors reveal that the predictions of Liu et al. (2001) model is producing estimates that are greater than number of cycle values determined by Seed et al. (1975) method. In the average, the difference is in the order of 5.5%.

On the other hand, Figures 4.26 to 4.28 present the assessments conducted for the field based weighting factor (i.e. m = 0.50). The residual plots along with their statistical descriptors reveal that the predictions of Liu et al. (2001) model is producing estimates that are greater than number of cycle values determined by Seed et al. (1975) method. In the average, the difference is in the order of 18.2%.

It should be noted that as the mean value of the residuals is getting closer to zero, the corresponding model is expected to produce more unbiased predictions, and a lower standard deviation means that the model produces more precise predictions. The calculated standard deviations of the residuals are in the order of 0.628, 0.630 and

0.631 for laboratory, average and field based models. These values, by themselves, may not be considered as a direct performance indicator but they will be used as a basis during comparison of Liu et al. (2001) original model with the revised version of it and also the other models developed as part of this study (the other models will be introduced in the following sections).

The calculated mean values of the residuals for each set indicate some degree of bias in predictions. Liu et al. (2001) mentioned that they used maximum likelihood methodology to determine their model coefficients; however, biased model predictions underlined the need of a re-visit to the proposed model. Following section will focus on re-assessment of Liu et al. model in the light of this study's database.

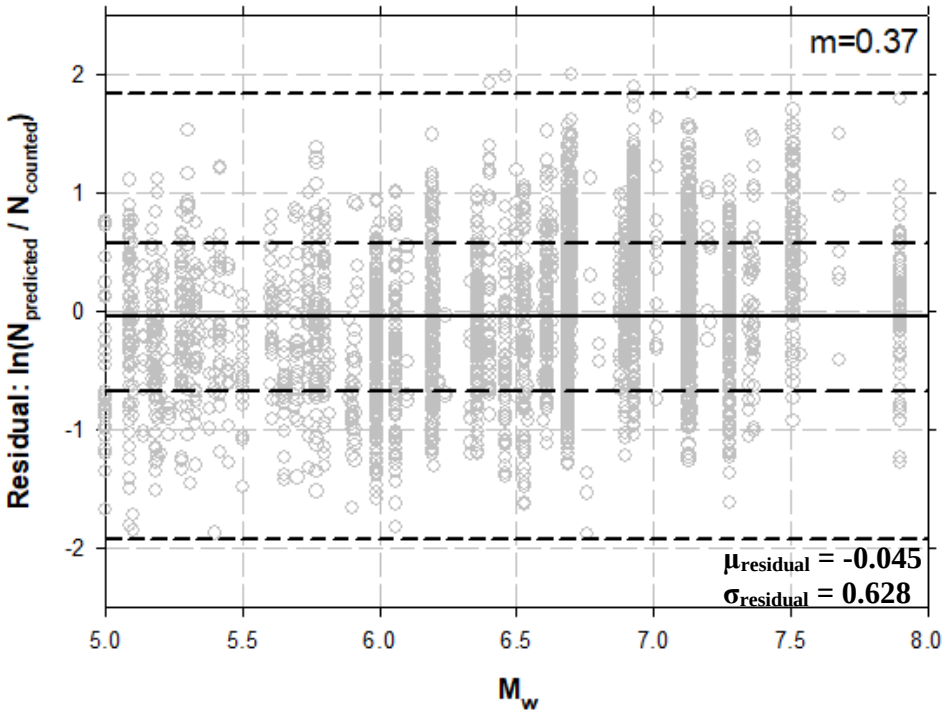

Figure 4.20. Residuals for Liu et al. (2001) model as a function of M_w - m=0.37

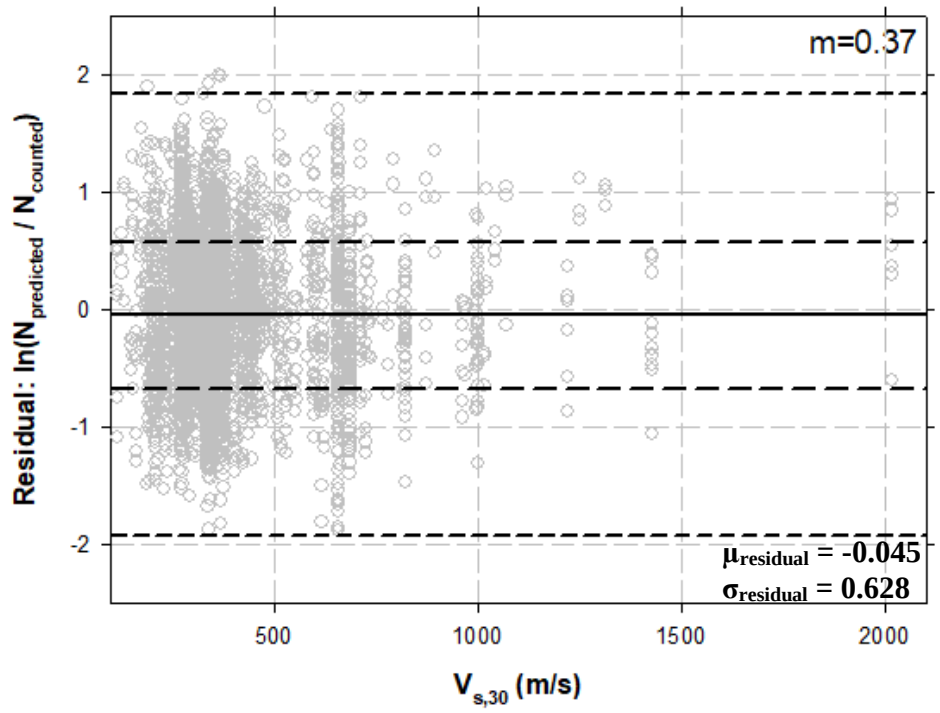

Figure 4.21. Residuals for Liu et al. (2001) model as a function of $V_{s,30}$ - m=0.37

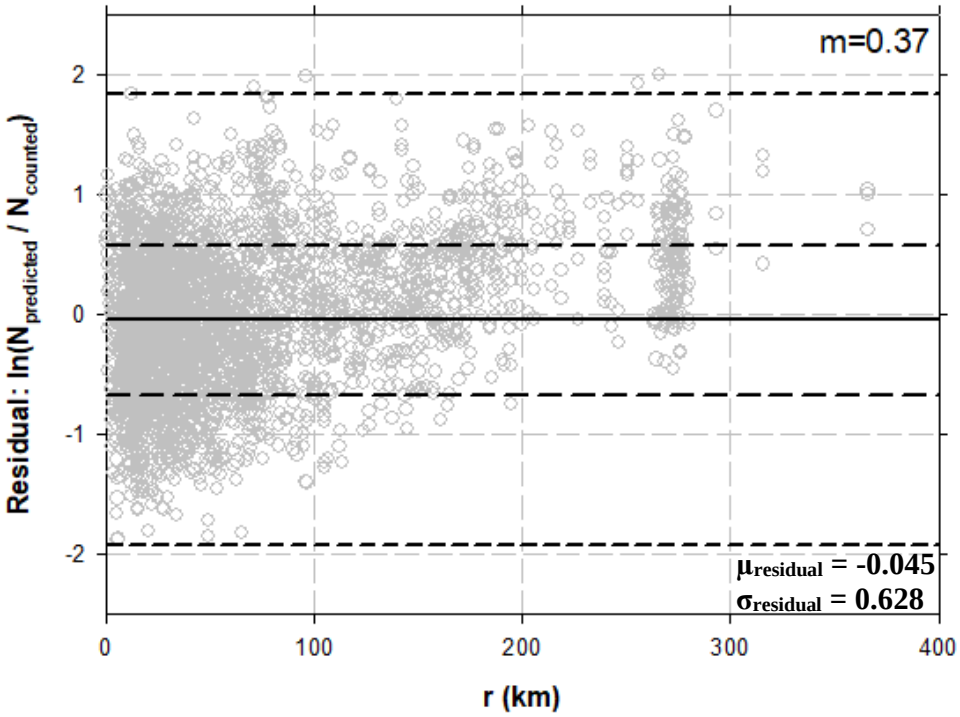

Figure 4.22. Residuals for Liu et al. (2001) model as a function of r - m=0.37

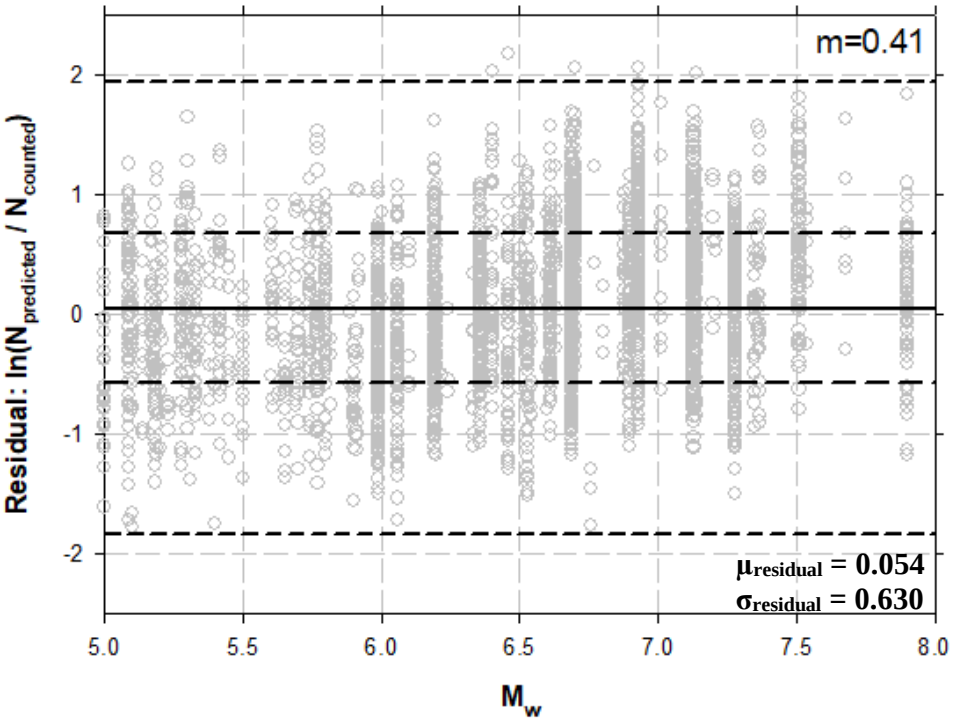

Figure 4.23. Residuals for Liu et al. (2001) model as a function of M_w - m=0.41

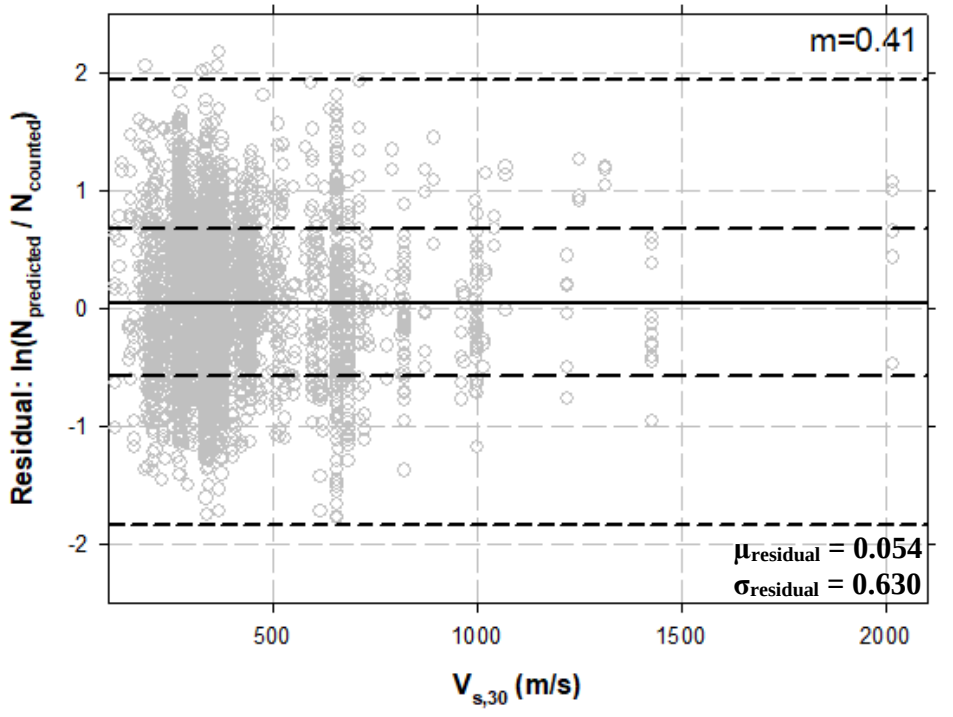

Figure 4.24. Residuals for Liu et al. (2001) model as a function of $V_{s,30}$ - m=0.41

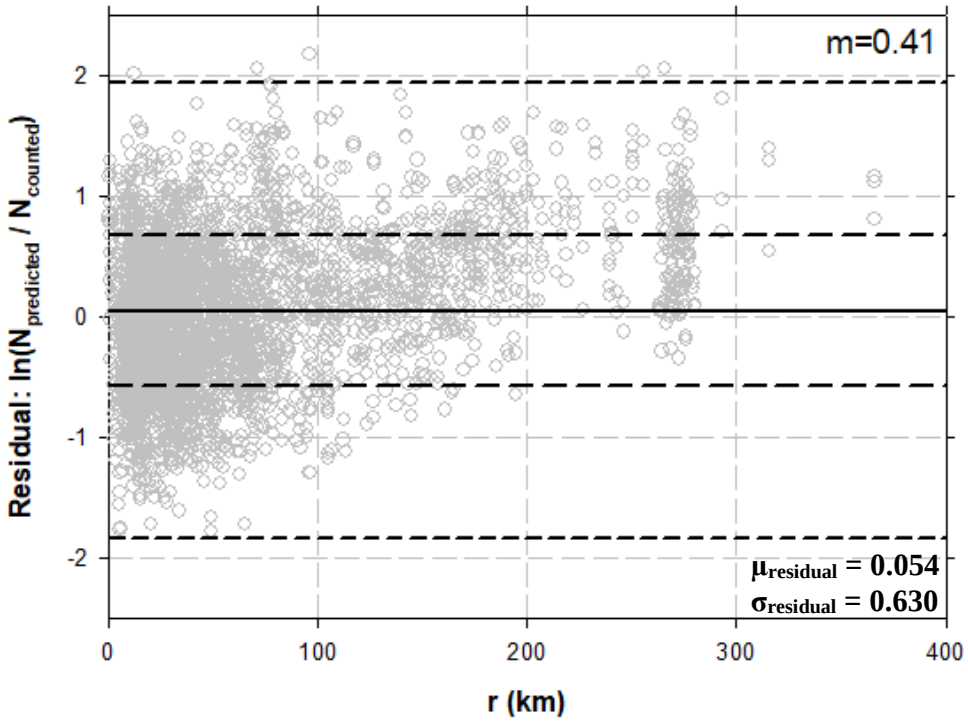

Figure 4.25. Residuals for Liu et al. (2001) model as a function of r- m=0.41

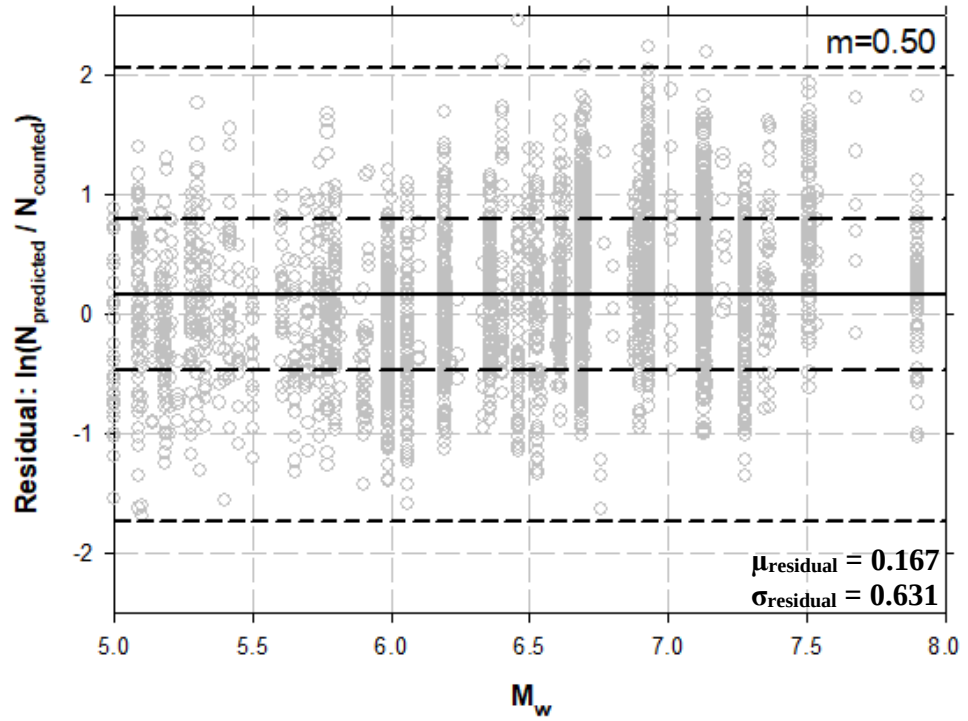

Figure 4.26. Residuals for Liu et al. (2001) model as a function of M_w - m=0.50

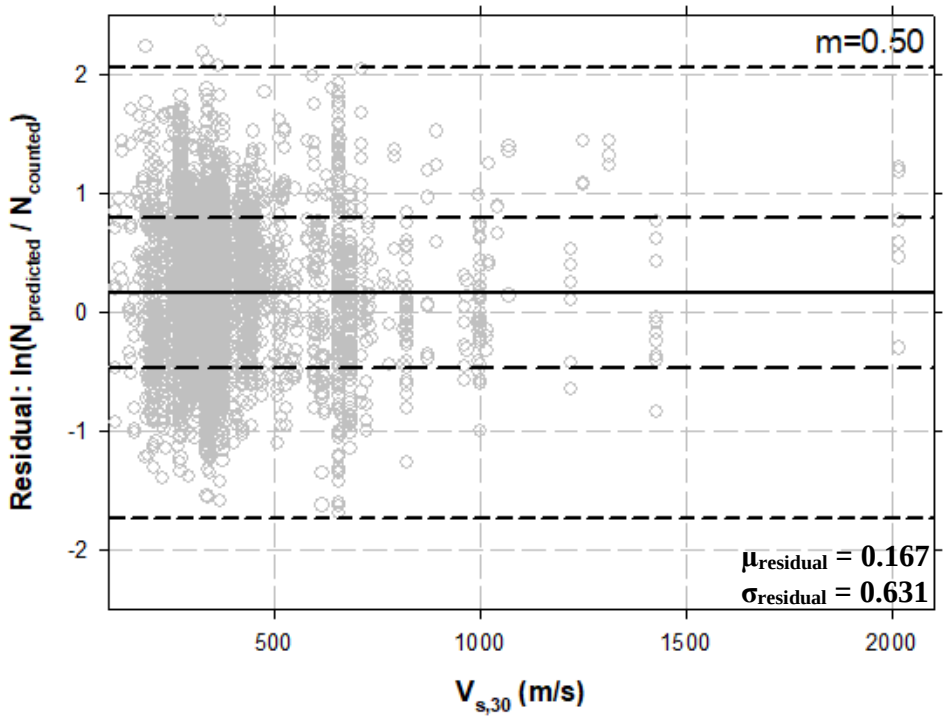

Figure 4.27. Residuals for Liu et al. (2001) model as a function of $V_{s,30}$ - m=0.50

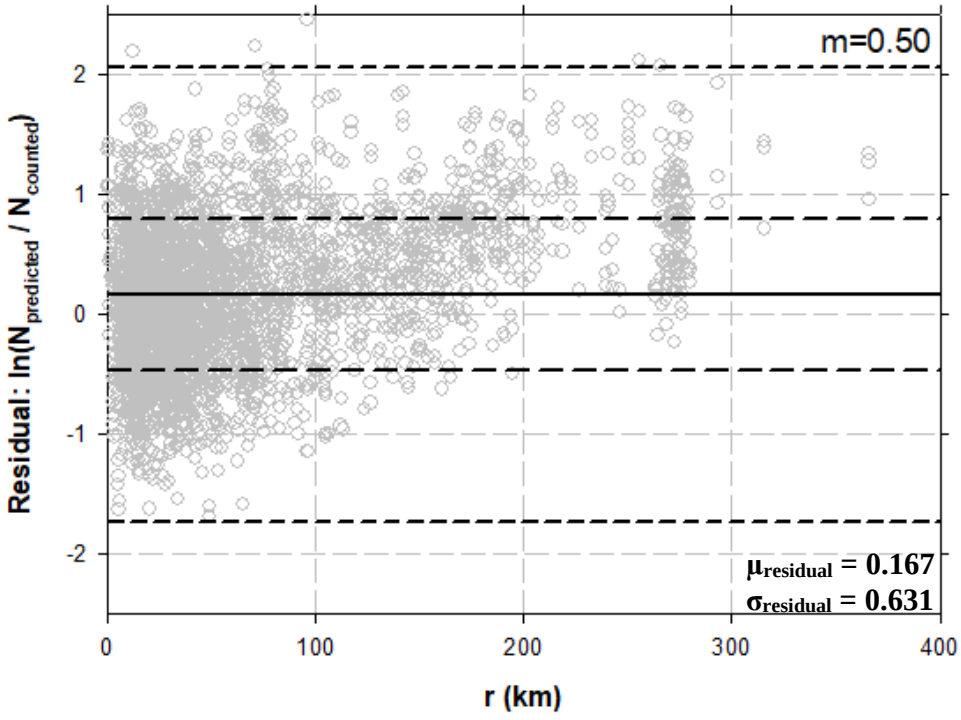

Figure 4.28. Residuals for Liu et al. (2001) model as a function of r- m=0.50

4.3.2. Performance Assessment of Revised Liu et al. (2001) Model

As mentioned in Section 4.3.1, Liu et al. (2001) model produces biased N predictions for the database formed as part of this study. For this reason, it is decided to re-evaluate the mathematical model recommended by Liu et al. (2001) by using the maximum likelihood methodology and this study's database. The revised coefficients for Liu et al. (2001) method are presented in Table 4.3 for selected weighting factors (i.e. 0.37, 0.41 and 0.50).

In order to evaluate the prediction performance of the revised model, residual plots were prepared as a function of important descriptive parameters (M_w, $V_{s,30}$ and r), and these plots are presented in Figures 4.29 to 4.37. As part of these plots the mean values of the residuals ($\mu_{residual}$) (by solid line) along with $\mu_{residual}\pm\sigma_{residual}$ (by medium dash line) and $\mu_{residual}\pm3\sigma_{residual}$ (by short dash line) are also presented to provide an insight on possible bias of the revised model.

Figures 4.29 to 4.31 present the assessments conducted for the laboratory based weighting factor (i.e. m=0.37). The residual plots along with their statistical descriptors reveal that the predictions of revised Liu et al. (2001) model is producing unbiased estimates in the average ($\mu_{residual} \sim 0.0$).

Figures 4.32 to 4.34 present the assessments conducted for the average case weighting factor (i.e. m=0.41). The residual plots along with their statistical descriptors reveal that the predictions of revised Liu et al. (2001) model is producing unbiased estimates in the average ($\mu_{residual} \sim 0.0$).

Figures 4.35 to 4.37 present the assessments conducted for the field based weighting factor (i.e. m=0.50). The residual plots along with their statistical descriptors reveal that the predictions of revised Liu et al. (2001) model is producing unbiased estimates in the average ($\mu_{residual} \sim 0.0$).

Aside from obtaining unbiased predictions in the average, it is also noted that standard deviation of the mean values of revised model also decrease from 0.628, 0.630 and

0.631 to 0.589, 0.591 and 0.588 for laboratory, average and field based weighting factors, respectively. Thus, it is concluded that this re-assessment study improves the Liu et al. (2001) model. However, based on the discussion presented in Section 4.1, it is concluded that the observed trends have not been fully incorporated in Liu et al. (2001) model; and consequently, there still exist a room for improvement in this research area.

Table 4.3. *Coefficients estimated by Liu (2001) and modified values*

Coefficients	Estimated by Liu (2001)	Modified Values
(a) Laboratory – based weighting factors		
b_1	1.89 ± 0.16	0.388
b_2	1.61 ± 0.13	2.353
c_1	0.668 ± 0.389	0.331
c_2	0.081 ± 0.013	0.026
Standard error	0.57	0.589
(b) Field – based weighting factors		
b_1	0.95 ± 0.14	-0.085
b_2	1.35 ± 0.12	2.249
c_1	0.93 ± 0.49	0.298
c_2	0.123 ± 0.016	0.031
Standard error	0.53	0.588
(c) Averaged weighting factors		
b_1	1.53 ± 0.15	0.256
b_2	1.51 ± 0.12	2.310
c_1	0.75 ± 0.42	0.323
c_2	0.095 ± 0.014	0.027
Standard error	0.56	0.591

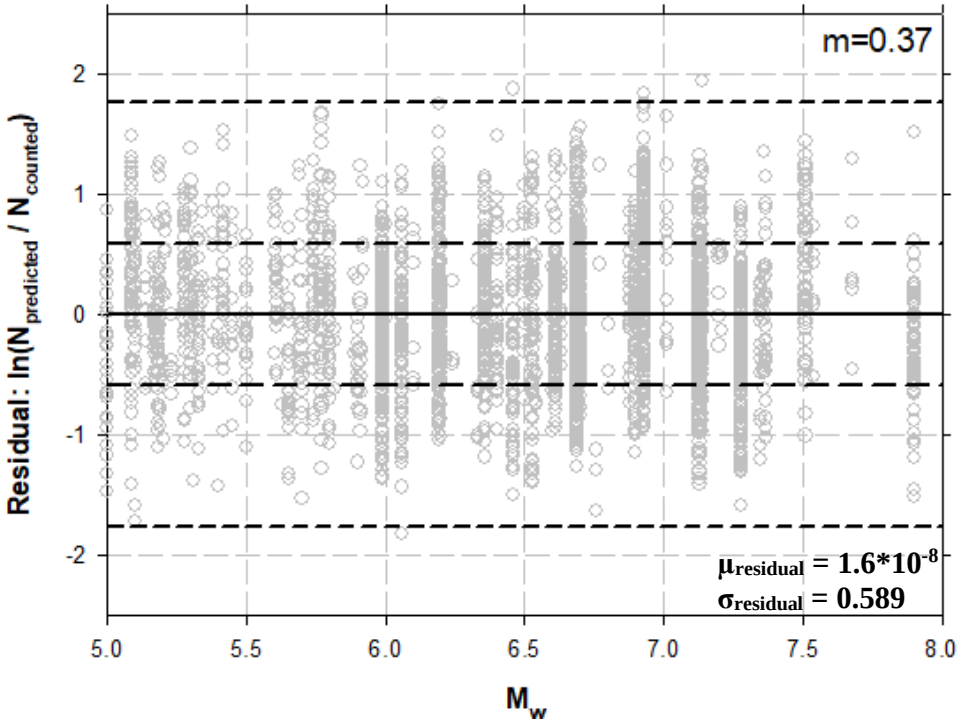

Figure 4.29. Residuals for revised Liu et al. (2001) model as a function of M_w - m=0.37

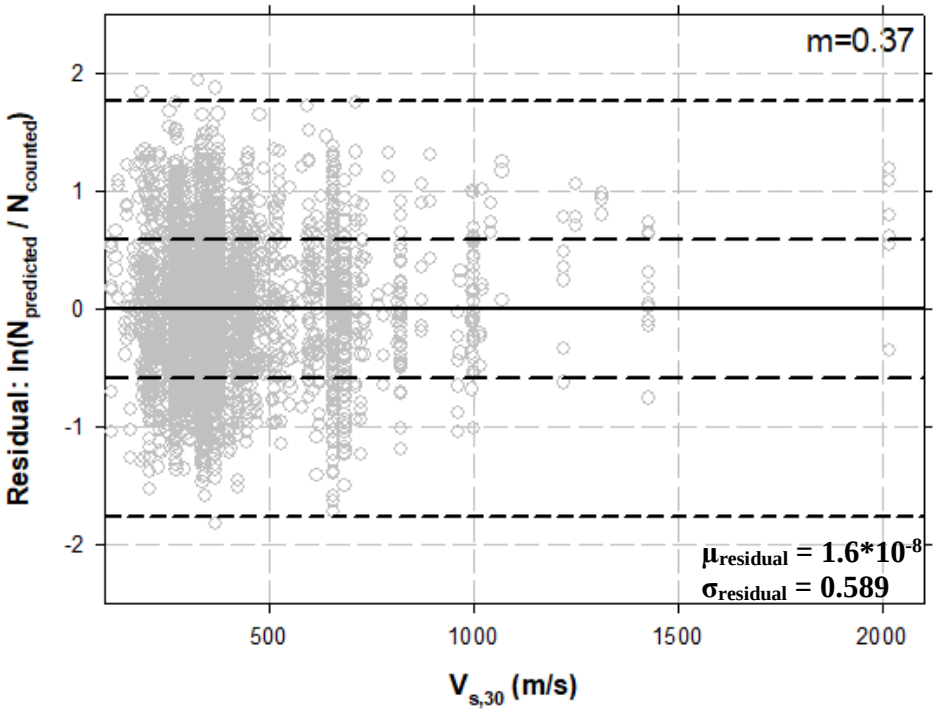

Figure 4.30. Residuals for revised Liu et al. (2001) model as a function of $V_{s,30}$ - m=0.37

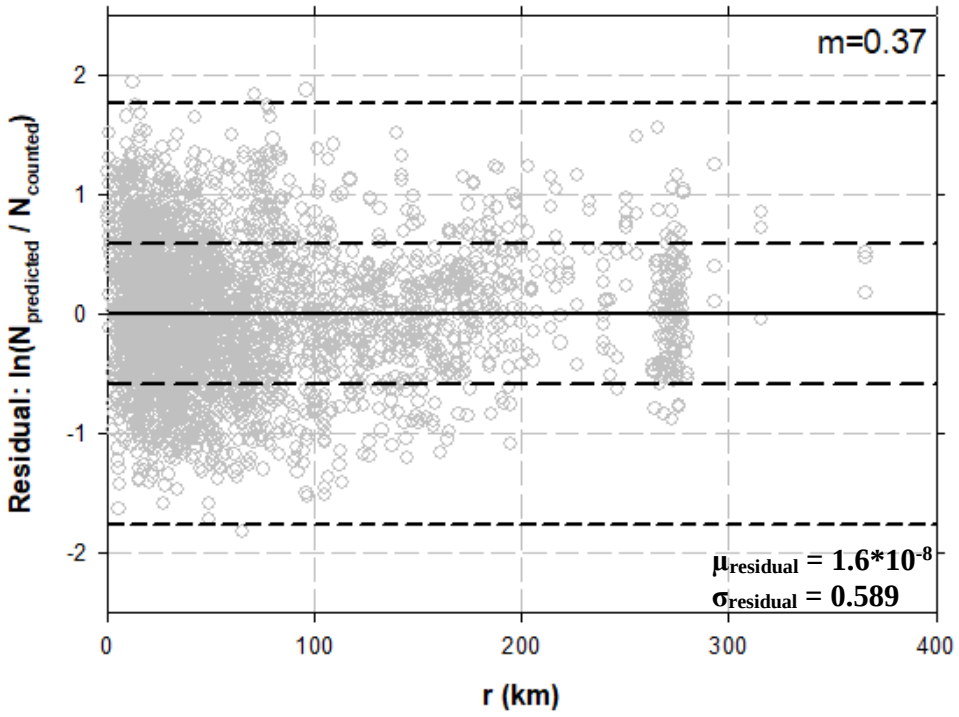

Figure 4.31. Residuals for revised Liu et al. (2001) model as a function of r - m=0.37

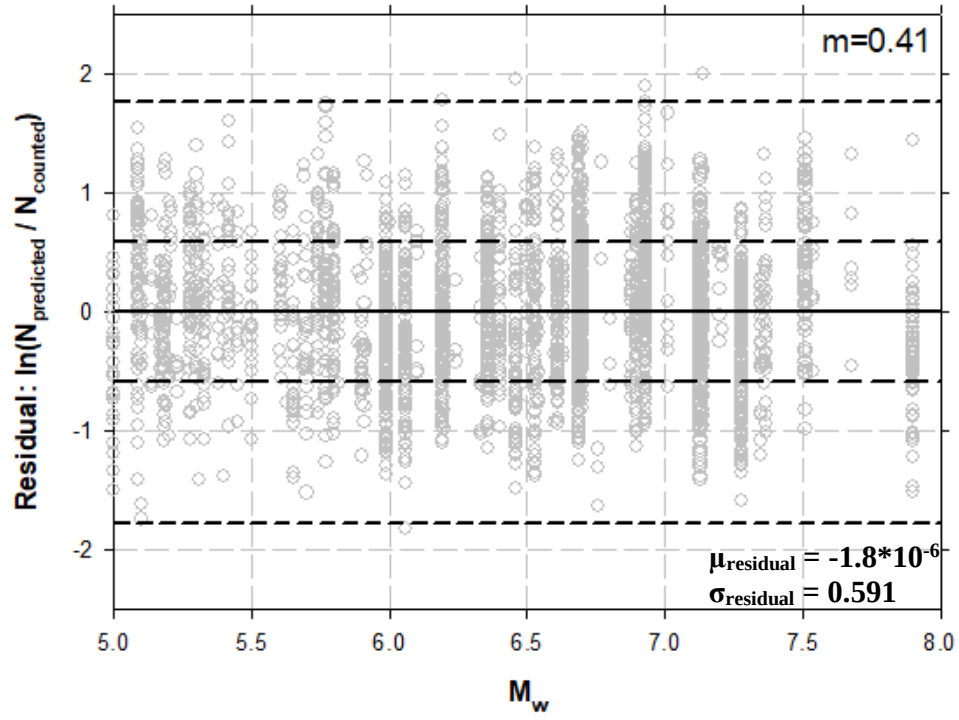

Figure 4.32. Residuals for revised Liu et al. (2001) model as a function of M_w - m=0.41

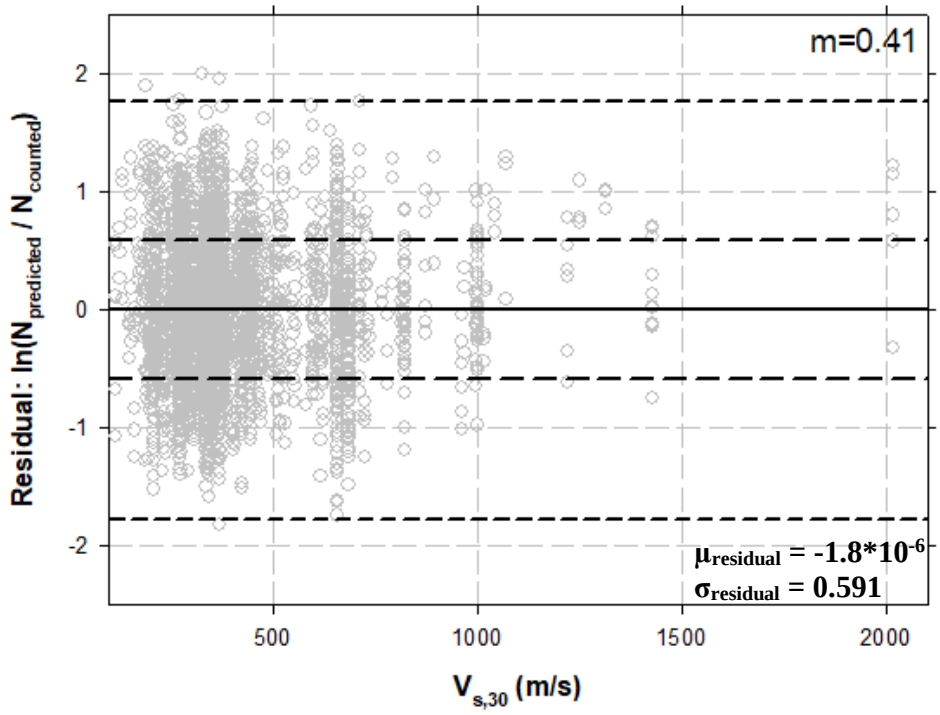

Figure 4.33. Residuals for revised Liu et al. (2001) model as a function of $V_{s,30}$ - m=0.41

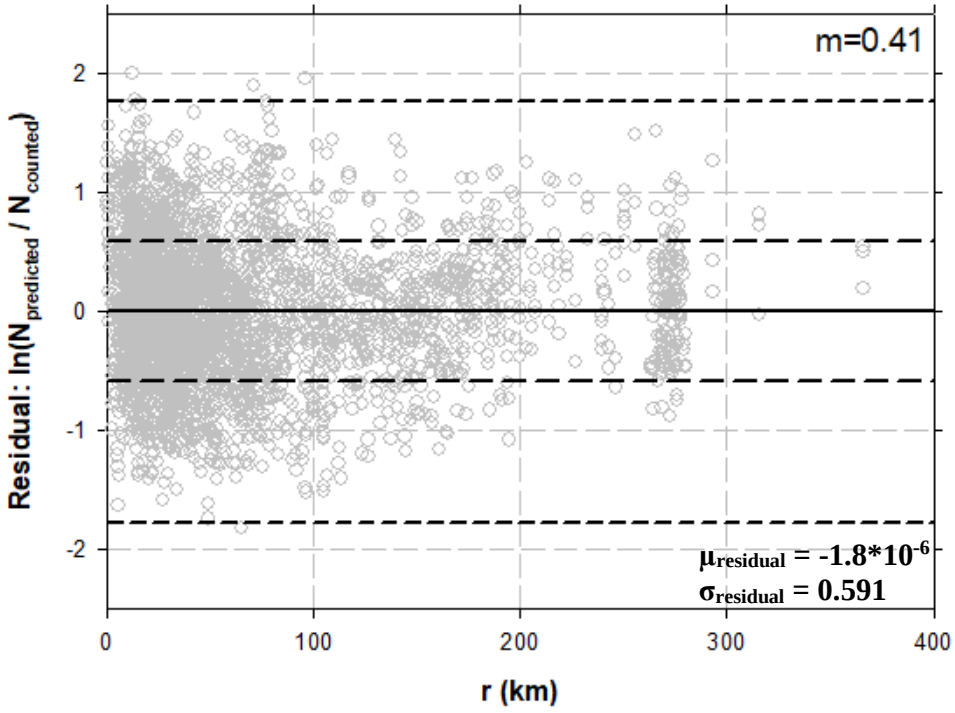

Figure 4.34. Residuals for revised Liu et al. (2001) model as a function of r - m=0.41

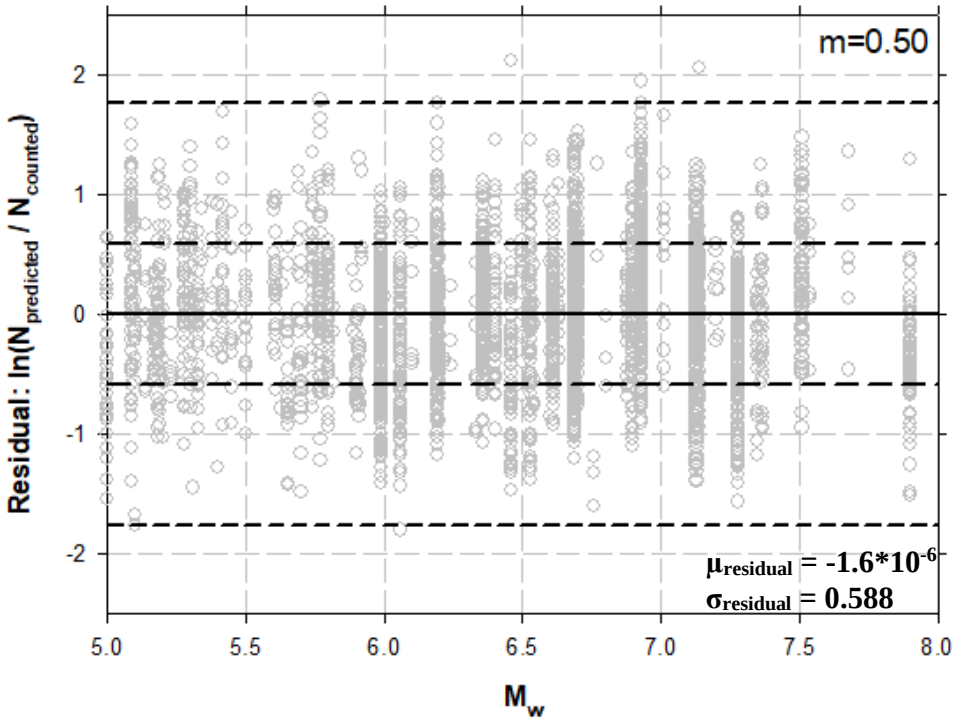

Figure 4.35. Residuals for revised Liu et al. (2001) model as a function of M_w - m=0.50

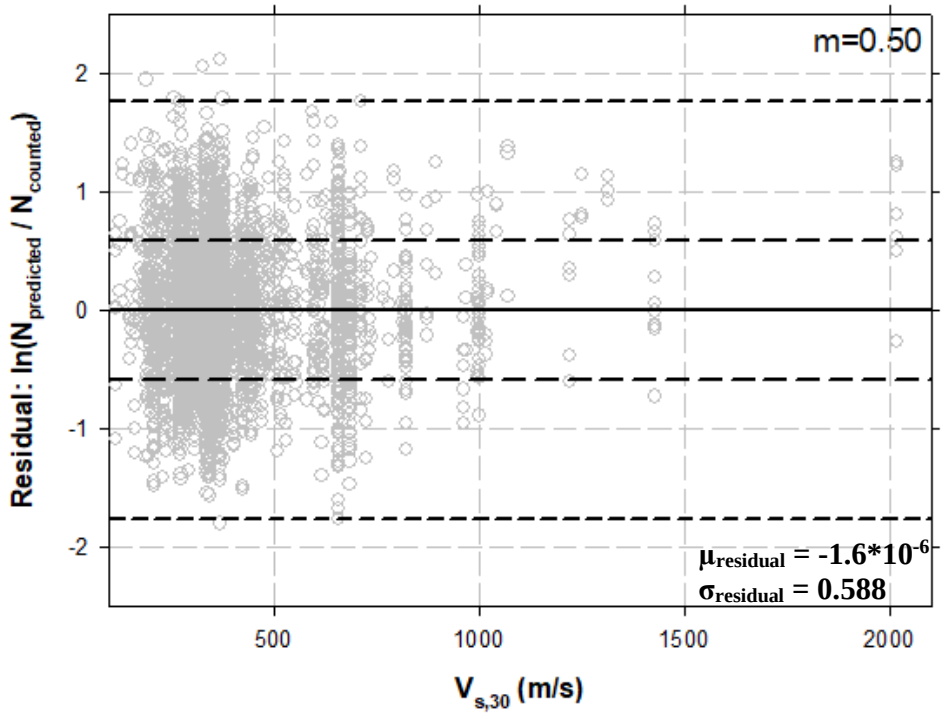

Figure 4.36. Residuals for revised Liu et al. (2001) model as a function of $V_{s,30}$ - m=0.50

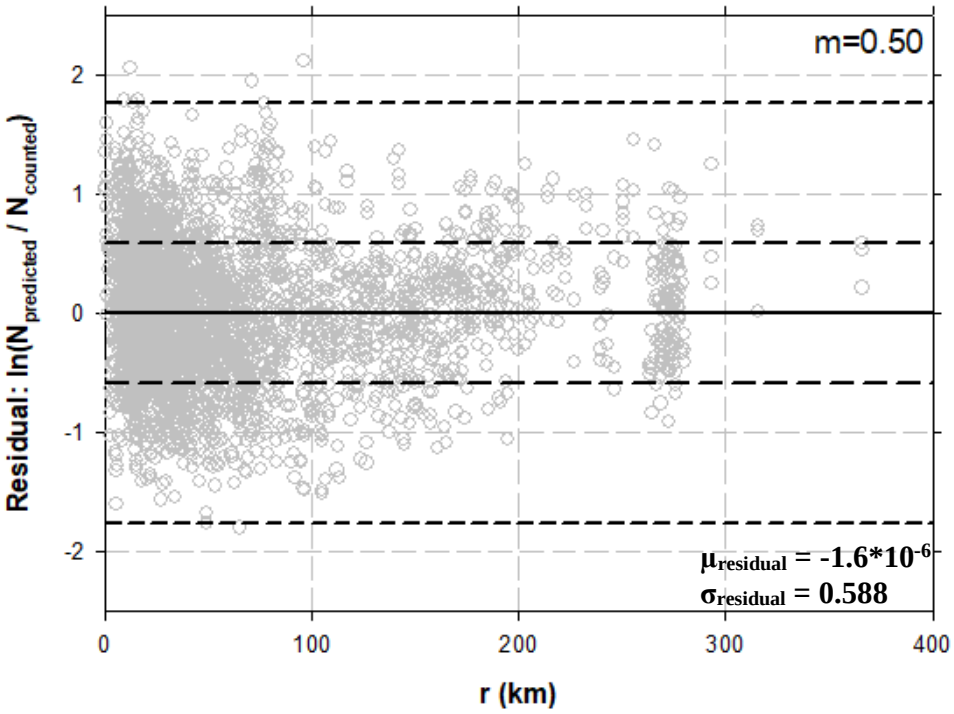

Figure 4.37. Residuals for revised Liu et al. (2001) model as a function of r- m=0.50

4.3.3. Performance New Equivalent Uniform Stress Cycle Model

The aim of this study is to develop a probability-based semi empirical model for estimation of number of equivalent uniform stress cycles for a given seismic scenario by taking into account earthquake, site and performance related variables such as the moment magnitude of earthquake (M_w), the site's representative shear wave velocity ($V_{s,30}$), site – source distance (R_{jb} and classification of whether it is near-, mid- or far-field site) and a performance criterion (weighting factor (m) can be defined in terms of a failure or performance criterion). This section is devoted to the introduction of these models and their products.

The first step in developing a probabilistic model is to develop a limit state expression that captures the essential parameters of the problem. The model for the limit state function has the general form g = g (**x, Θ**) where x is a set of descriptive parameters and Θ is the set of unknown model parameters. Inspired by data trends summarized below and presented thoroughly in Section 4.2, various functional forms were tested.

- N increases as M_w increases
- N has an increasing trend with increasing m, but this trend also depends on the increase of M_w
- ln (N) increases as R_{jb} increases
- ln (N) decreases as $V_{s,30}$ increases

Based on these general trends, various functional forms were analyzed and some of them are listed in Table 4.4. Among these, the following function (Equation 4.4) produced the best fit to the observed trends and adopted as the main limit state function of this study:

$$\ln\left(N_{predicted}\right) = \ln\left(f_1(M_w) * f_2(m)\right) - f_3\left(R_{jb}, V_{s,30}\right) + f_4\left(R_{jb}\right) \quad (4.4a)$$

$$\ln(N) = \ln\left(N_{predicted}\right) \pm \sigma_\varepsilon \quad (4.4b)$$

where $f_1(M_w)$ is the moment magnitude dependence, $f_2(m)$ is the weighting factor dependence, $f_3(R_{jb}, V_{s,30})$ is the site-source distance and site characteristic dependence and $f_4(R_{jb})$ is the distance dependence. Aside from these components, the proposed model includes a random model correction term (ε) to account for the facts that possible missing descriptive parameters with influence on number of uniform equivalent stress cycles may exist and / or the adopted mathematical expression may not have the ideal functional form. It is reasonable and also convenient to assume that ε has normal distribution with zero mean for the aim of producing an unbiased model (i.e., one that in the average makes correct predictions). The standard deviation of ε, denoted as σ_ε, however is unknown and must be estimated. As will be subsequently illustrated, data scatter is observed to be reduced by increasing Joyner-Boore distance (R_{jb}) values. Thus, model uncertainty is preferred to be a function of "R_{jb}". This suggests a heteroscedastic σ_ε mode as expressed in Equation in 4.5. Then, the set of unknown parameters of the model becomes $\Theta = (\boldsymbol{\theta}, \sigma_\varepsilon)$.

$$\sigma_\varepsilon = \frac{1}{{R_{jb}}^{\theta_{11}} + \theta_{12}} \quad (4.5)$$

Within the scope of this chapter, these functions will be developed according to previous studies and the distribution graphs presented in previous chapters.

Table 4.4. *Alternative mathematical expressions for number of equivalent uniform stress cycle*

Trial #	Mathematical Expressions	σ_ε
1	$\ln(N) = \ln\left(f_1(M_w) * f_2(m)\right) - f_3\left(R_{jb}, V_{s,30}\right)$	Constant
2	$\ln(N) = \ln\left(f_1(M_w) * f_2(m)\right) - f_3\left(R_{jb}, V_{s,30}\right) + f_4\left(R_{jb}\right)$	Constant
3	$\ln(N) = \ln\left(f_1(M_w) * f_2(m)\right) - f_3\left(R_{jb}, V_{s,30}\right) + f_4\left(R_{jb}\right)$	Variable

The first component of Equation 4.4 is $f_1(M_w)$ which is the magnitude dependence function. This component of the proposed model is adopted from the mathematical expression proposed by Liu et al. (2001) considering its special features that were discussed in detail as part of Chapter 2. For the sake of completeness, the related functional form is presented in Equation 4.6.

$$f_1(M_w) = \frac{\left(\frac{\exp(\theta_1 + \theta_2(M_w - M_w^*))}{10^{1.5M_w + 16.05}}\right)^{-\frac{1}{3}}}{4.9 * 10^6 \beta} \tag{4.6}$$

where θ_1 and θ_2 are model coefficients, β is the shear wave velocity at the source which is usually taken as 3.2 km/s (Liu et al., 2001), M_w is the moment magnitude and M_w^* is the reference moment magnitude (this parameter will also be assessed in maximum likelihood assessments but it is preferred to represent this parameter as M_w^* rather than referring it as θ_i).

The second component of Equation 4.4 is $f_2(m)$ which is the weighting factor dependence function. As presented in Figure 4.4, N is dependent to both m and M_w. As M_w's subsequent effects are taken into account in $f_1(M_w)$, after various trials in terms of limit state functions it is decided not to incorporate M_w into $f_2(m)$ expression. To exclude the effect of M_w from this component, a normalization scheme, similar to the one followed by Cetin and Bilge (2012) for development of their performance based (i.e. m-dependent) magnitude scaling factors, is used. The first step of this scheme includes binning the existing database in terms of M_w (5.0 – 5.5, 5.5 – 6.0,

6.0- 6.5, 6.5 – 7.0 and 7.0 – 8.0). The average of counted N values is calculated for each weighting factor (m), and this step is repeated for each M_w bin separately. Per recommendations of Liu et al. (2001), m = 0.41 is accepted as the average value, and calculated averages of counted N values are normalized to $N_{m=0.41}$ value for each M_w bin. In addition, as mentioned in Section 4.1, number of cycles decrease up to approximately 0.25 but after this point N values tend to increase as the weighting factor increases. Therefore, m values of less than 0.25 were not used to better represent the distribution of N and m. The resulting normalized curves for different M_w bins are presented in Figure 4.38 along with a trend line that covers the whole $N / N_{m=0.41}$ vs. m relations.

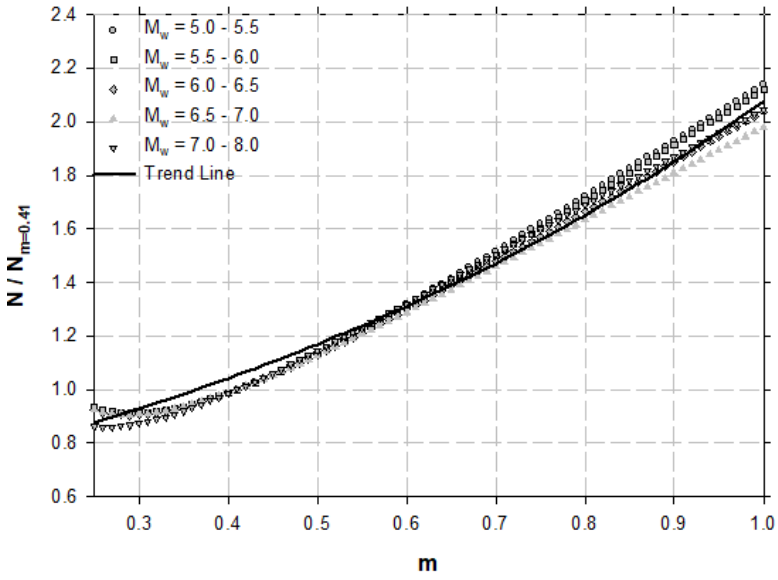

Figure 4.38. Relationship between normalized number of cycle and weighting factor for different moment magnitude ranges

The trend line presented in Figure 4.38 that correlates m and N will constitute the basis of $f_2(m)$ formulation, and weighting factor-based component is expressed as given in Equation 4.7.

$$f_2(m) = \theta_3 * \exp(\theta_4 * m) \tag{4.7}$$

It should be noted this function is directly in the form of the trend line presented in Figure 4.38, and it can be expressed as given in Equation 4.8.

$$f_2(m) = 0.658 * \exp(1.15 * m) \quad (4.8)$$

0.658 and 1.15 will be the initial estimates ofθ_3 and θ_4, respectively and these coefficients will be evaluated in maximum likelihood analysis.

The third component of Equation 4.4 is $f_3(R_{jb}, V_{s,30})$ which is defined as a function of the site - source distance and site characteristics. As mentioned in Section 4.1, N depends on both site - source distance (in terms of R_{jb}) and site characteristics (in terms of $V_{s,30}$). However, they have opposite effects on N, i.e. N increases with increasing R_{jb}, but N decreases with increasing $V_{s,30}$. In order to evaluate this issue, a unified field classification system has been introduced as discussed in Section 4.1.1. The database trends are presented in terms of N – $V_{s,30}$ and N – R_{jb} plots for the sites classified as near-, mid- and far-field in Section 4.1.2, and it can be observed from Figures 4.11 to 4.19 that the slope of the trend lines vary for each class. In order to quantify the relation between N and $V_{s,30}$, a normalization scheme similar to the one used for N and m is needed. Normalization for the N – m relationship is conducted in terms of m; however, this time the normalization is conducted in terms of Joyner-Boore distance (R_{jb}). It should be noted that the sites are classified as near-, mid- and far-fields according to r_{near} and r_{far}, and consequently the normalization is decided to be defined separately for each field class. For this reason, a normalized distance index (τ) function is introduced for assessment of each field class as presented in Equation 4.9.

$$\tau = \begin{cases} \theta_9 * \dfrac{R_{jb}}{r_{near}} & near\ field \\ \theta_9 + (\theta_{10} - \theta_9) * {(R_{jb} - r_{near})}\Big/{(r_{far} - r_{near})} & mid\ field \\ \theta_{10} * \dfrac{R_{jb}}{r_{far}} & far\ field \end{cases} \quad (4.9)$$

By incorporating this normalized distance index, the third component of the proposed model is formulated as given in Equation 4.10.

$$f_3(R_{jb}, V_{s,30}) = (\theta_5 * \tau^{\theta_6} + \theta_7) * V_{s,30} \quad (4.10)$$

where θ_5, θ_6 and θ_7 are model coefficients, and the normalized distance index (τ) is also defined in terms of two other model coefficients (θ_9 and θ_{10}) and $V_{s,30}$ is the representative shear wave velocity of the top 30 m.

The last component of the model is $f_4(R_{jb})$ the site - source distance dependent function. This function was developed to describe the effect of the R_{jb} on N. After analyzing various mathematical expressions, the function given in Equation 4.11 is decided to be used.

$$f_4(R_{jb}) = \begin{cases} \theta_8 * \mathrm{R_{jb}} & R_{jb} \leq 1 \\ \theta_8 * \log(R_{jb}) & R_{jb} > 1 \end{cases} \quad (4.11)$$

In the light of this discussion, the functional forms given in Table 4.4 are presented in detail in Table 4.5. The main difference between Trials 2 and 3 are about incorporation of a heteroscedastic σ_ε model.

Table 4.5. *Mathematical forms of alternative models*

Trial #	Mathematical Forms
1*	$\ln(N) = \ln\left(\frac{\left(\frac{\exp(\theta_1+\theta_2(M_w-M_w{}^*))}{10^{1.5M_w+16.05}}\right)^{-\frac{1}{3}}}{4.9*10^6\beta} * \theta_3 * \exp(\theta_4 * m)\right) - \left(\theta_5 * \tau^{\theta_6} + \theta_7\right) * V_{s,30}$
2*	$\ln(N) = \ln\left(\frac{\left(\frac{\exp(\theta_1+\theta_2(M_w-M_w{}^*))}{10^{1.5M_w+16.05}}\right)^{-\frac{1}{3}}}{4.9*10^6\beta} * \theta_3 * \exp(\theta_4 * m)\right) - \left(\theta_5 * \tau^{\theta_6} + \theta_7\right) * V_{s,30} + \theta_8 * \log(R_{jb})$
3**	$\ln(N) = \ln\left(\frac{\left(\frac{\exp(\theta_1+\theta_2(M_w-M_w{}^*))}{10^{1.5M_w+16.05}}\right)^{-\frac{1}{3}}}{4.9*10^6\beta} * \theta_3 * \exp(\theta_4 * m)\right) - \left(\theta_5 * \tau^{\theta_6} + \theta_7\right) * V_{s,30} + \theta_8 * \log(R_{jb})$

* Model correction term is defined as a constant
** Model correction term is defined as a function of r

4.3.4. Maximum Likelihood Assessments

This section is devoted to the results of maximum likelihood analyses for the alternative models presented in Table 4.5. Details of formulation of the likelihood function are presented in Appendix B. Consistent with this methodology, model coefficients are estimated by maximizing the likelihood functions given in Table 4.5. The estimated model coefficients and calculated summation of likelihood values ($\sum lh$) are presented in Table 4.6.

Table 4.6. *Summary of model coefficients and likelihood values of trials*

Trial #	Model Coefficients														$\sum lh$
	θ_1	θ_2	M_w^*	θ_3	θ_4	θ_5	θ_6	θ_7	θ_8	θ_9	θ_{10}	θ_{11}	θ_{12}	σ_ε	
1	4.19	3.06	5.68	2.1	2.8	0.0079	0.128	0.00316	-	0.0001	0.001	-	-	0.86	-83836
2	2.20	2.31	5.68	0.907	1.32	0.0075	0.076	0.002	6.78	0.00012	0.000141	-	-	0.591	-54194
3	2.20	2.31	5.68	0.907	1.32	0.00858	0.1177	0.00309	6.94	0.00011	0.00024	0.0422	0.658	-	-53815

As the results of probabilistic analyses indicate, the functional form given by Trial #3 has higher likelihood value ($\sum \mathbf{lh}$) than others. Thus, it is concluded that this model produces relatively the best predictions compared to the other alternatives. The predictive performance of the proposed model will be discussed in the next chapter.

CHAPTER 5

PREDICTIVE PERFORMANCE OF THE PROPOSED MODEL

5.1. Introduction

As introduced within the confines of Section 4.2.3 and 4.2.4, various limit state models were developed and tested to estimate the equivalent number of stress cycles for given earthquake, site and performance related parameters. After testing various alternatives, a heteroscedastic σ_ε model is determined to produce the best fit to observed behavioral trends. The proposed model is presented in Equation 5.1.

$$ln(N) = ln\left(\frac{\left(\frac{exp(2.2+2.31(M_w-5.68))}{10^{1.5M_w+16.05}}\right)^{-\frac{1}{3}}}{4.9*10^6\beta} * 0.907 * exp(1.32*m)\right) - (0.00858*\tau^{0.1177}+0.00309)*V_{s,30}+6.94*log(R_{jb}) \quad (5.1)$$

The power of the proposed mathematical form (i.e. limit state function) is also assessed by simple statistics (i.e. mean and standard deviation) of residuals (i.e. ln ($N_{predicted}$ / $N_{counted}$).

For the proposed model, the variation of the residuals as a function of model parameters, M_w, R_{jb}, $V_{s,30}$ and m are presented in Figures 5.1, 5.2, 5.3 and 5.4, respectively. Since standard deviation is function of r, the calculated mean and standard deviation of the residuals are also presented in Figure 5.3. In the figure, the mean values of the residuals ($\mu_{residual}$) (by solid line), $\mu_{residual}\pm\sigma_{residual}$ (by medium dash line) and $\mu_{residual}\pm3\sigma_{residual}$ (by short dash line) are also plotted to provide an insight on the precision of the proposed model.

For the whole database, the mean value of the residuals is 0.026 which means that predictions of the model are 2.6% higher than the counted N values according to the

Seed et al. (1975) method. The resulting mean residual is considered to be low enough and it is concluded that the proposed model provides unbiased estimates of N. Aside from it on these figures; a constant standard deviation for residual values is presented. As given in Equation 5.1, the standard deviation of the error function is defined as a function of R_{jb} but in order to provide a basis to compare the standard deviation of the proposed model with other estimation methods (such as original Liu et al. (2001), revised Liu et al. or the alternatives tested as part of Section 4.2.3), the average of the calculated standard deviations of residuals was determined and reported on these figures. Only for Figure 5.3, which presents the variation of residuals as a function of R_{jb}, different R_{jb} ranges are defined and their corresponding $\mu_{residual}$ and $\sigma_{residual}$ values are reported separately to highlight the R_{jb} dependence of the proposed model. As Figure 5.3 implies, a larger scatter is observed at $R_{jb} < 100$ km as $\sigma_{residual}$ value is higher than the overall constant $\sigma_{residual}$ of the model.

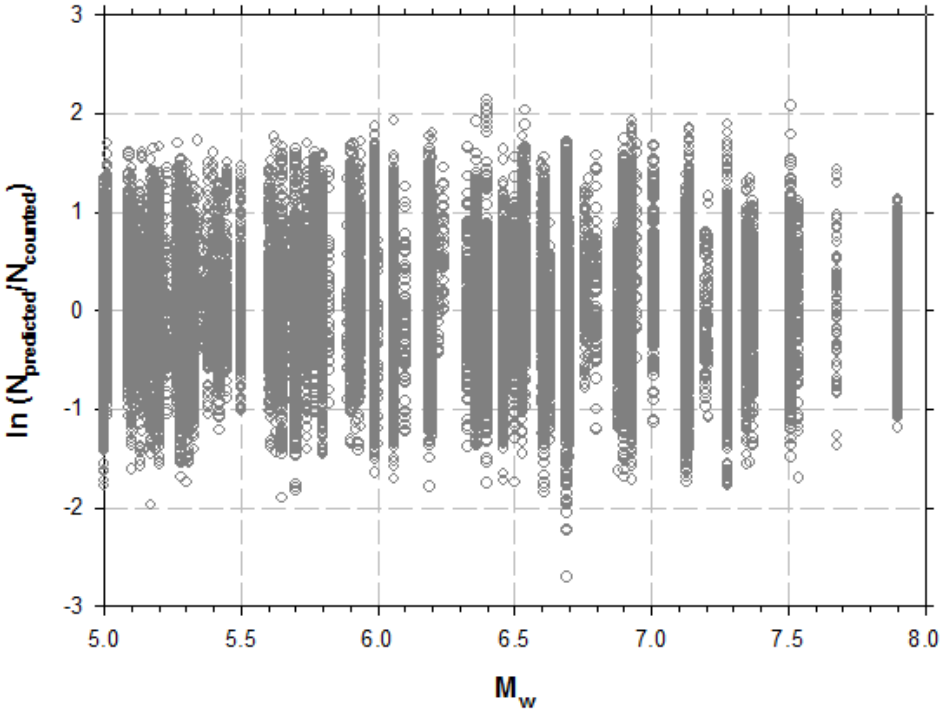

Figure 5.1. Residuals for the proposed model as a function of M_w

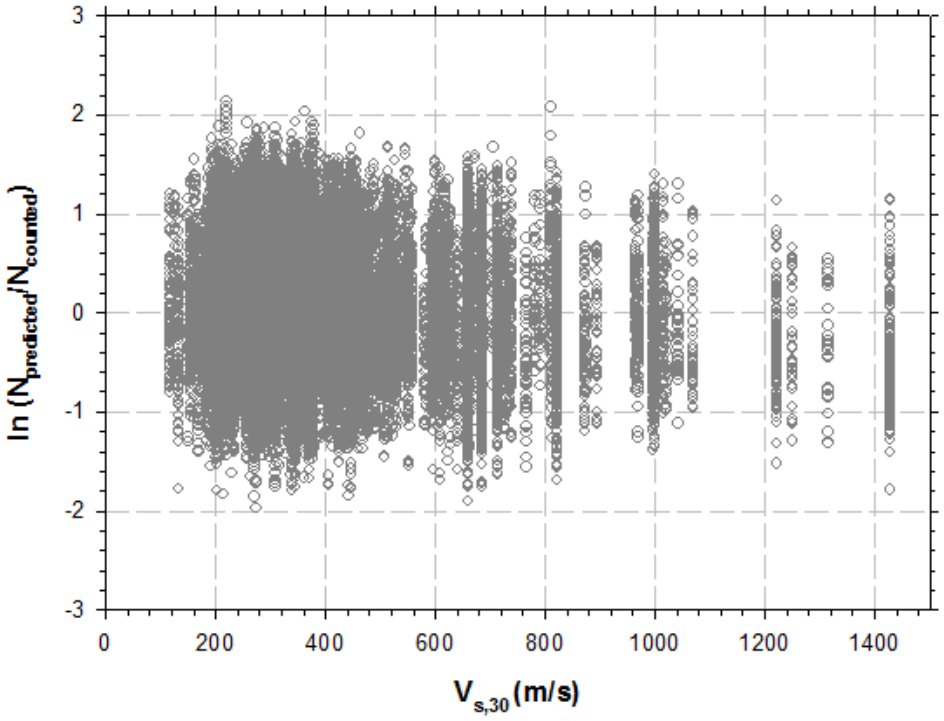

Figure 5.2. Residuals for the proposed model as a function of $V_{s,30}$

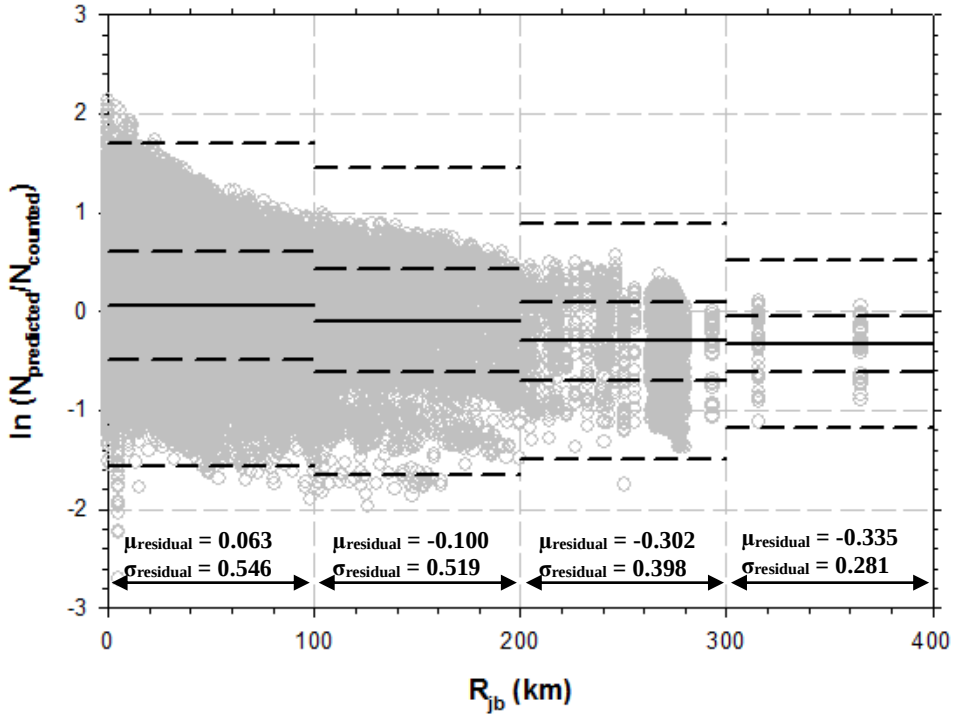

Figure 5.3. Residuals for the proposed model as a function of R_{jb}

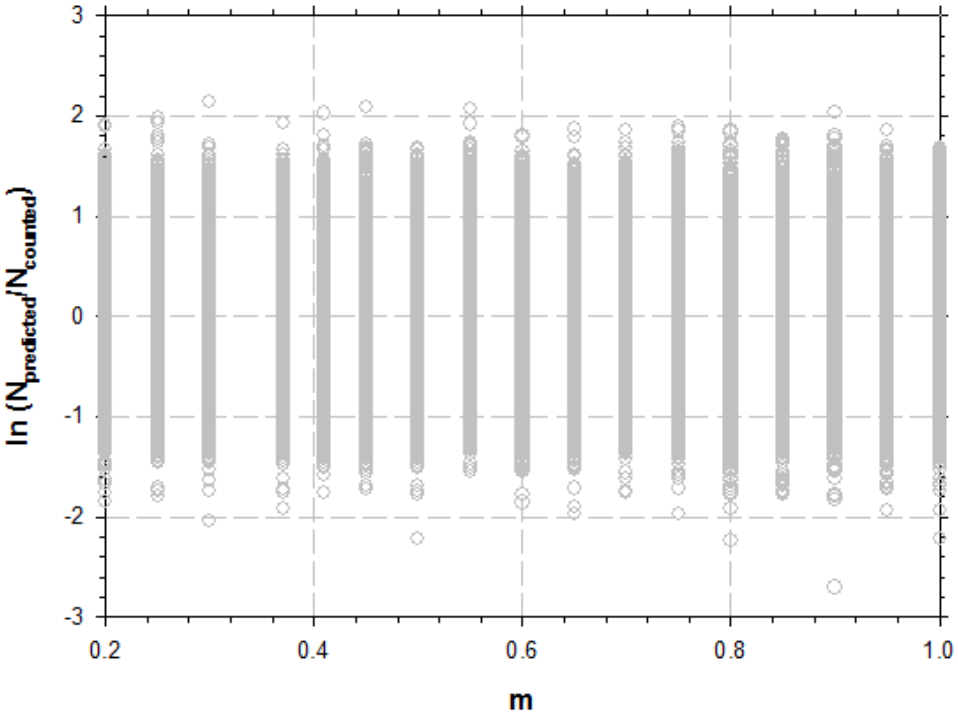

Figure 5.4. Residuals for the proposed model as a function of m

CHAPTER 6

SUMMARY AND CONCLUSION

6.1. Summary

Assessment of cyclic (seismic) response of soils is considered to be one of the most challenging research topics in geotechnical earthquake engineering. Over the last 6 decades, many researchers have focused on this topic either by using earthquake case history, or laboratory or field experiment approaches. In the latter approaches, as opposed to the random and irregular (transient) nature of earthquake waves, cyclic loading is generally applied in a uniform manner (in the form of sine or cosine waves) to the reconstituted (or undisturbed) soil samples. Thus, this approach requires a conversion scheme. In their pioneer study, Seed et al. (1975) proposed a method to represent an irregular stress time history by equivalent uniform stress series. Following this benchmark study, the earliest efforts to estimate the equivalent number of uniform stress cycles for a given earthquake magnitude were mostly judgmental. Yet in time, more advanced and sophisticated approaches have been proposed. However, a critical review of the existing literature has revealed that; i) currently, a significantly extended earthquake record catalogs exists, which enables better assessment of cyclic stress conversions of irregular transient earthquake records to harmonic uniform stress cycles, and ii) based on the argument proposed by Cetin and Bilge (2012), weighting factor of conversion relationships are now known to be strain dependent. Hence, a revisit to the whole concept is believed to be needed. Inspired by these research opportunities, it is intended to develop semi-empirical model for estimation of equivalent number of uniform stress cycles as a function of earthquake, site and performance parameters.

The purpose of this thesis was to develop robust probability-based semi-empirical models for the prediction of equivalent number of stress cycles of a scenario earthquake event defined by earthquake magnitude, distance to source mechanism, soil site properties and selected performance (shear strain) criteria. Considering the above listed limitations of earlier efforts and significance of the issue, a comprehensive research study was performed. For the purpose of compiling an extended database, Pacific Earthquake Engineering Research Center's earthquake catalog (www.peer.berkeley.edu) has been extensively studied. 4176 records from 90 earthquakes, from 1935 Helena, Montana Earthquake to 2002 Denali, Alaska Earthquake were evaluated within this scope. The reported moment magnitudes for these earthquakes vary in the range of 5.0 to 7.9. The representative shear wave velocities ($V_{s,30}$) of the measurement stations from which the acceleration times histories were obtained are reported to vary from 116.35 m/s to 2016.13 m/s; whereas, their Joyner-Boore distances vary in the range of 0 km to 365.14 km to the seismic source. By following the cycle counting scheme of Seed et al. (1975), all of these acceleration time histories were evaluated by taking into account 17 different weighting factors varying in the range of 0.2 to 1.0 considering the recommendations of Cetin and Bilge (2012). These efforts result in a database having a total of 74,970 data points as presented thoroughly in Appendix – A.

The database trends were carefully studied as discussed in Chapters 3 and 4 to assess trends between N - M_w, $V_{s,30}$, R_{jb} and m. Using the existing trends as the starting point, the relationship was quantified by following a probabilistic framework. Maximum likelihood methodology was followed to determine, the model coefficients of the evaluated model alternatives. Relatively the most superior predictive model that produces unbiased predictions (i.e. accurate) with highest degree of precision (i.e.: the smallest model error standard deviation) is determined based on these probabilistic assessments.

6.2. Conclusion

Considering its relation with intensity and duration of strong ground motions, earthquake magnitude is a vital parameter for geotechnical earthquake engineering assessments. While case history based approaches can directly use magnitude, it is not possible in experimental efforts. Thus, robust methods for conversion from earthquake magnitude to equivalent uniform stress cycles are in need. Many researchers have worked on this topic. Especially, the recommendations of Seed et al. (1975) have served to the geotechnical earthquake engineering community for more than two decades. Moreover, the cycle counting scheme proposed by that research still constitutes the basis of this kind of studies. Later, Liu et al. (2001) developed empirical relationships between N and M_w, site – source distance, site conditions and factors representing near-fault rupture directivity effects. On the other hand, this study has been in extensive use for the last 2 decades. However, considering the limits of its database along with the issues highlighted within the confines of this thesis, it is intended to evaluate Liu et al. (2001) and proposed a better alternative, if possible.

By following maximum likelihood methodology, the original proposal of Liu et al. (2001) was evaluated (Section 4.2.1). Considering the bias in its predictions, by keeping the same mathematical form its model coefficients were re-evaluated and a relatively more accurate and precise model was reached as presented in Section 4.2.2. Then, by considering all the variables of this complex problem, alternative models were developed as introduced in 4.2.3. These models were evaluated by maximum likelihood assessments. All of the evaluated models are summarized in Table 6.1 for the sake of completeness.

Table 6.1. *Proposed predictive models*

Model #	Mathematical Forms
1*	$\ln(N) = \ln\left(\frac{\left(\frac{\exp(4.19+3.06(M_w-5.68))}{10^{1.5M_w+16.05}}\right)^{-\frac{1}{3}}}{4.9*10^6\beta} * 2.1 * \exp(2.8*m)\right) - (0.00079*\tau^{0.128} - 0.00316) * V_{s,30}$
2*	$\ln(N) = \ln\left(\frac{\left(\frac{\exp(2.2+2.31(M_w-5.68))}{10^{1.5M_w+16.05}}\right)^{-\frac{1}{3}}}{4.9*10^6\beta} * 0.907 * \exp(1.32*m)\right) - (0.0075*\tau^{0.076} + 0.002) * V_{s,30} + 6.78 * \log(R_{jb})$
3**	$\ln(N) = \ln\left(\frac{\left(\frac{\exp(2.2+2.31(M_w-5.68))}{10^{1.5M_w+16.05}}\right)^{-\frac{1}{3}}}{4.9*10^6\beta} * 0.907 * \exp(1.32*m)\right) - (0.00858*\tau^{0.1177} + 0.00309) * V_{s,30} + 6.94 * \log(R_{jb})$

A comparative study in terms of both the summation of likelihood function along with simple statistical descriptors (in terms of mean and standard deviation of residuals along with Pearson product moment correlation coefficient (R^2)) is performed as presented in Table 6.2.

Table 6.2. *A summary of predictive model performances*

Model	$\mu_{residual}$	$\sigma_{residual}$	R^2	$\sum lh$
Liu et al. (2001)	-0.045*	0.628*	0.16*	-3,040**
Revised Liu et al. (2001)	**-1.6*10^{-6}***	0.588*	0.18*	-3,031**
Trial #1	0.403	0.860	0.16	-83,836***
Trial #2	0.021	**0.54**	**0.34**	-54,194***
Trial #3	0.026	**0.54**	**0.34**	**-53,815***

***The best of those calculated for three different m values is presented**
****Total of calculated likelihoods of 3,415 data**
*****Total of calculated likelihood of 66,307 data**

A careful inspection of Table 6.2 implies that the proposed model (Equation 6.1), the proposed model (referred as Model #3 in Table 6.1) produces satisfactorily the most unbiased response with the highest degree of precision, the use of which is recommended for the assessment of equivalent number of stress cycles conversion for weighting factor equal or greater than 0.25.

REFERENCES

REFERENCES

Boore, D. M. (1983). Stochastic simulation of high-frequency ground motions based on seismological model of the radiated spectra. *Bull. Seismological Soc. Of Am*., *73*(6), 1865-1894.

Boore, D. M. & Atkinson G. M. (2008). Ground-Motion Prediction Equations for the Average Horizontal Component of PGA, PGV, and 5%-Damped PSA at Spectral Periods between 0.01 *s* and 10.0 *s*. *Earthquake Spectra: February 2008*, Vol. 24, No. 1, pp. 99-138.

Brune, J.N. (1970). Tectonic stress and the spectra of seismic shear waves from earthquakes. *J. Geophysical Research*, 75, 4997-5009.

Brune, J.N. (1971). Correction. *J. Geophysical Research*, 75, 5002.

Cetin, K. O., and Bilge, H. T. (2012). Cyclic large strain and induced pore pressure models for saturated clean sands. *J. Geotech. Geoenviron. Eng*., *138*(3), 309–323.

Cetin, K. O., et al. (2004). "SPT-based probabilistic and deterministic assessment of seismic soil liquefaction potential." *J. Geotech. Geoenviron. Eng.*, *130*(12), 1314–1340.

DeAlba, P., Chan, C., & Seed, H. B. (1975). Determination of soil liquefaction characteristics by large-scale tests. *Rep. No. EERC 75-14*, Earthquake Engineering Research Center, Univ. of CA, Berkeley, CA.

Green, R. A., & Terri, G. A. (2005). Number of equivalent cycles concept for liquefaction evaluations—Revisited. J. *Geotech. Geoenviron. Eng.*, *131*(4), 477–488.

Hanks, T.C., and Kanamori, H. (1979). A moment magnitude scale. *J. Geophy. Res.*, 84, 2348-2350.

Hanks, T.C., and McGuire, R.K. (1981). The character of high frequency strong ground motion. *Bull. Seism. Soc. Am*., 71, 2071-2095.

Hansen, W.R. (1965). Effects of the earthquake of March 27, 1964, at Anchorage, Alaska: U.S. *Geological Survey Professional Paper* 542-A, p. A1-A68.

Idriss, I. M. (1997). Evaluation of liquefaction potential and consequences: Historical perspective and updated procedure. *Presentation Notes, 3rd Short Course on Evaluation and Mitigation of Earthquake Induced Liquefaction Hazards*, San Francisco.

Kramer S. L. and Elgamal A. W. (2001). Modeling Soil Liquefaction Hazards for Performance-Based Earthquake Engineering, *PEER Report 2001/13*, Earthquake Engineering Research Center, University of California, Berkeley.

Lee, K. L. & Chan, K. (1972). Number of equivalent significant cycles in strong motion earthquakes. *Proc. of the International Conference on Microzonation for Safer Construction Research and Application*, Seattle Washington, pp. 609-627.

Liu, A. H. (2001). Equivalent number of uniform stress cycles for soil liquefaction analysis. *MS thesis*, Dept. Of Civ. Engrg., University of California, Los Angeles.

Liu, A. H., Stewart, J. P., Abrahamson, N. A., & Moriwaki, Y. (2001). Equivalent number of uniform stress cycles for soil liquefaction analysis. *J. Geotech. Geoenviron. Eng.*, *127*(12), 1017–1026.

Marcuson, (1978). Definition of terms related to liquefaction. *J. Geot. Div., ASCE 104*, GT9.

Seed, H. B., & Idriss, I. M. (1971). Simplified procedure for evaluating soil liquefaction potential. *J. Soil Mech. Found. Div.*, *97*(9), 1249–1273.

Seed, H. B., & Idriss, I. M. (1982). Ground motion and soil liquefaction during earthquakes. *Earthquake Engineering Res. Institute Monograph*, Oakland, CA.

Seed, H. B., Idriss, I. M., Makdisi, F., & Banerjee, N. (1975). Representation of, irregular stress time histories by equivalent uniform stress series in liquefaction analysis. *Rep. No. EERC75-29*, Earthquake Engineering Research Center, College of Engineering, Univ. of CA, Berkeley, CA.

Seed, R. B., Cetin, K. O., Moss, R. E. S., Kammerer, A. M., Wu, J., Pestana, J. M., Riemer, M. F., Sancio, R. B., Bray, R. B., Kayen, R. E. & Faris, A. (2003). Recent advances in soil liquefaction engineering: a unified and consistent framework, *Report No. EERC 2003-06*, Earthquake Engineering Research Center, University of California, Berkeley.

Somerville, P.G., Smith, N.F., Graves, R.W., & Abrahamson, N.A. (1997). Modification of empirical strong ground motion attenuation relations to include the amplitude and duration effects of rupture directivity. *Seism. Res. Letters, 68*(1), 199222.

Youd, T.L. and Noble, S.K. (1997) Magnitude Scaling Factors. *NCEER Workshop on Evaluation of Liquefaction Resistance of Soils*, National Center for Earthquake Engineering Research, State University of New York at Buffalo, 149-165

APPENDICES

A. Summary of The Database

Table A.1. *Earthquakes used in this study*

Earthquake	Year	Magnitude
ABRUZZO	1984	5.80
ANZA	1980	5.19
AQABA	1995	7.20
BAJA	1987	5.50
BIGBEAR	1992	6.46
BORAH.AS	1983	5.10
BORAH.MS	1983	6.88
BORREGO	1942	6.50
BORREGO	1968	6.63
CABAJA	2002	5.31
CALDIRAN	1976	7.21
CAPEMEND	1992	7.01
CHALFANT	1986	5.44
CHALFANT	1986	5.65
CHALFANT	1986	5.77
CHALFANT	1986	6.19
COALINGA	1983	5.09
COALINGA	1983	5.18
COALINGA	1983	5.21
COALINGA	1983	5.23
COALINGA	1983	5.38
COALINGA	1983	5.77
COALINGA	1983	6.36

Table A.1 Continued

Earthquake	Year	Magnitude
CORINTH	1981	6.60
COYOTELK	1979	5.74
CTRCALIF	1954	5.30
CTRCALIF	1960	5.00
DENALI	2002	7.90
DINAR	1995	6.40
DOUBSPRG	1994	5.90
DURSUN.BEY	1979	5.34
DUZCE	1999	7.14
ELALAMO	1956	6.80
ERZIKAN	1992	6.69
FRIULI	1976	5.50
FRIULI	1976	5.91
FRIULI	1976	6.50
GAZLI	1976	6.80
GEORGIA	1991	6.20
GREECE	1980	5.20
GREECE	1983	6.70
GREECE	1984	5.00
GREECE	1984	5.30
GREECE	1985	5.20
GREECE	1986	5.40
GREECE	1986	6.20
GREECE	1990	6.10
GULFCA	2001	5.70
HECTOR	1999	7.13
HELENA	1935	6.00
HOLLISTR	1961	5.50

Table A.1 Continued

Earthquake	Year	Magnitude
HOLLISTR	1961	5.60
HOLLISTR	1974	5.14
HOLLISTR	1986	5.45
HUMBOLT	1937	5.80
IMPVALL	1938	5.00
IMPVALL	1940	6.95
IMPVALL	1951	5.60
IMPVALL	1953	5.50
IMPVALL	1955	5.40
IMPVALL	1979	5.01
IMPVALL	1979	5.62
IMPVALL	1979	6.53
ITALY	1979	5.90
ITALY	1980	6.20
ITALY	1980	6.90
IZMIR	1977	5.30
KERN	1952	7.36
KOBE	1995	6.90
KOCAELI	1999	7.51
KOZANI	1995	5.10
KOZANI	1995	5.30
KOZANI	1995	6.40
LANDERS	1992	7.28
LIVERMOR	1980	5.42
LIVERMOR	1980	5.80
LOMAP	1989	6.93
LYTLECR	1970	5.33
MAMMOTH	1980	5.69

Table A.1 Continued

Earthquake	Year	Magnitude
MAMMOTH	1980	5.70
MAMMOTH	1980	5.91
MAMMOTH	1980	5.94
MAMMOTH	1980	6.06
MAMMOTH	1983	5.31
MAMMOTH	1983	5.34
MANAGUA	1972	5.20
MANAGUA	1972	6.24
MANJIL	1990	7.37
MOHAWK	2001	5.17
MORGAN	1984	6.19
MTLEWIS	1986	5.60
NAHANNI	1985	6.76
NCALIF	1941	6.40
NCALIF	1952	5.20
NCALIF	1954	6.50
NCALIF	1960	5.70
NCALIF	1967	5.20
NCALIF	1967	5.60
NCALIF	1975	5.20
NENANA	2002	6.70
NEWZEAL	1984	5.50
NEWZEAL	1987	5.80
NEWZEAL	1987	6.60
NEWZEAL	1992	5.70
NORTH001	1994	6.05
NORTH009	1994	5.20
NORTH142	1994	5.93

Table A.1 Continued

Earthquake	Year	Magnitude
NORTH151	1994	5.13
NORTH392	1994	5.28
NORTHR	1994	6.69
NWCALIF	1938	5.50
NWCALIF	1941	6.60
NWCALIF	1951	5.80
NWCHINA1	1997	5.90
NWCHINA2	1997	5.93
NWCHINA3	1997	6.10
NWCHINA4	1997	5.80
OROVILLE	1975	5.89
PALMSPR	1986	6.06
PARKF	1966	6.19
PTMUGU	1973	5.65
ROERMOND	1992	5.30
ROUNDVAL	1984	5.82
SANFRAN	1957	5.28
SANJUAN	1998	5.17
SANSALV	1986	5.80
SBARB	1978	5.92
SCALIF	1952	6.00
SFERN	1971	6.61
SITKA	1972	7.68
SKULLMT	1992	5.65
SMADRE	1991	5.61
SMART1	1981	5.90
SMART1	1983	6.50
SMART1	1985	5.80

Table A.1 Continued

Earthquake	Year	Magnitude
SMART1	1986	6.32
SMART1	1986	7.30
SPITAK	1988	6.77
STELIAS	1979	7.54
SUPERST	1987	6.22
SUPERST	1987	6.54
TABAS	1978	7.35
TRINIDAD	1980	7.20
TRINIDAD	1983	5.70
UPLAND	1990	5.63
VICT	1980	6.33
WESTMORL	1981	5.90
WHITTIER	1987	5.27
WHITTIER	1987	5.99
YOUNTVL	2000	5.00

B. Details of Formulation of The Likelihood Function

The first step in developing a probabilistic model is to develop a limit state expression that captures the essential parameters of the problem. The model for the limit state function has the general form $\delta = g(x,\Theta)$ where x is a set of descriptive parameters and Θ is the set of unknown model parameters. Inspired by data trends as presented in Chapter 3 and 4, various functional forms were tested as presented in Chapter 4, Table 4.4.

Among these, the following expression has produced the best fit to the observed trends, and it is consequently selected as the limit state function for estimation of

number of equivalent uniform stress cycles (N), where θ_i represents the set of unknown model coefficients:

$$\delta_N(M_w, r, V_{s,30}, m, \Theta) = \ln(N) - \left\{ \ln\left[\frac{\left(\frac{\exp(\theta_1+\theta_2(M_w-M_{w^*}))}{10^{1.5M_w+16.05}}\right)^{-1/3}}{4.9*10^6\beta} * (\theta_3 * \exp(\theta_4 * m)) \right] - (\theta_5 * \tau^{\theta_6} + \theta_7) * V_{s,30} + \theta_8 * \log(R_{jb}) \right\} \pm \varepsilon_{\gamma_N} \quad (B.1)$$

where M_w, R_{jb}, $V_{s,30}$ and m are moment magnitude, Joyner-Boore distance, representative V_s of the top 30 m of the project site and weighting factor, respectively; whereas τ is defined as given in Equation B.2.

$$\tau = \begin{cases} \theta_9 * \dfrac{R_{jb}}{r_{near}} & for\ near\ fields; i.e.\ R_{jb} \le r_{near} \\ \theta_9 + (\theta_{10} - \theta_9) * {(R_{jb} - r_{near})}/{(r_{far} - r_{near})} & for\ mid\ fields; i.e.\ r_{near} \le R_{jb} \le r_{far} \\ \theta_{10} * \dfrac{R_{jb}}{r_{far}} & for\ far\ fields; i.e.\ r_{far} \le R_{jb} \end{cases} \quad (B.2)$$

where r_{near} and r_{far} are defined as given in Equations B.3 and B.4, respectively.

$$r_{near} = 0.5 * e^{\frac{2.37 - M_W}{\ln(V_{s,30})}} \quad (B.3)$$

$$r_{far} = 85 * e^{\frac{0.4 * M_W}{\sqrt{\ln(V_{s,30})}}} \quad (B.4)$$

The proposed model includes a random model correction term (ε) to take into account i) possible missing descriptive parameters having an effect on N may exist, and ii) the selected functional form may not be the ideal form. It is reasonable and convenient to assume that ε has normal distribution with zero mean for the aim of producing an unbiased model. However, standard deviation of the error term (σ_ε) is unknown and must be estimated. As discussed in Chapter 4, data scatter is observed to be reduced by increasing Joyner-Boore distance (R_{jb}). Thus it is preferred to define the σ_ε as a function of r; i.e. using a heteroscedastic model as expressing in Equation B.5. Then the set of the model will be $\Theta = (\theta, \sigma_\varepsilon)$.

$$\sigma_{\varepsilon_{\ln(N)}} = \frac{1}{R_{jb}\theta_{11} + \theta_{12}} \quad (B.5)$$

Assuming that each N data is statistically independent, the likelihood function for "n" cases can be written as the product of the probabilities of the observations.

$$L_N(\theta,\sigma_\varepsilon)=\prod_{i=1}^{n}P\left[\left(\delta_N\left(M_{w,i},R_{jb,i},V_{s,30,i},m_i,\theta\right)=0\right]\right. \qquad (B.6)$$

Suppose the values of $M_{w,i}$, $R_{jb,i}$, $V_{s,30,i}$, m_i, and N_i at the each data point are exact, i.e. no measurement error exists, noting that $\delta(..)=\hat{\delta}(...)+\varepsilon_i$ has the normal distribution with mean $\hat{\delta}$ and standard deviation σ_ε. Then the likelihood function can be written as a function of unknown coefficients as in Equation B.7, where φ [.] is the standard normal probability density function.

$$L_N(\theta,\sigma_\varepsilon)=\prod_{i=1}^{n}\varphi\left[\frac{\hat{\delta}_N(M_{w,i},R_{jb,i},V_{s,30,i},m_i,N_i,\theta)}{\sigma_N}\right] \qquad (B.7)$$

consistent with the maximum likelihood methodology, model coefficients are estimated by maximizing the function given in Equation B.7. These coefficients are presented in Table B.1.; whereas the final form of the proposed model is presented in Equation B.8 along with ± 1 standard deviation range.

$$ln\left(N_{predicton}\right)=ln\left(\frac{\left(\frac{exp(2.2+2.31(M_w-5.68))}{10^{1.5M_w+16.05}}\right)^{-\frac{1}{3}}}{4.9*10^6\beta}*0.907*exp(1.32*m)\right)$$
$$-(0.00858*\tau^{0.1177}+0.00309)*V_{s,30}+6.94*log\left(R_{jb}\right)\pm\frac{1}{{R_{jb}}^{\theta_{11}}+\theta_{12}} \qquad (B.8a)$$

$$\tau=\begin{cases}0.00011*\dfrac{R_{jb}}{r_{near}} & for\ near\ fields;i.e.\ R_{jb}\le r_{near}\\ 0.00011+(0.00024-0.00011)*{\left(R_{jb}-r_{near}\right)}/{\left(r_{far}-r_{near}\right)} & for\ mid\ fields;i.e.\ r_{near}\le R_{jb}\le r_{far}\\ 0.00024*\dfrac{R_{jb}}{r_{far}} & for\ far\ fields;i.e.\ r_{far}\le R_{jb}\end{cases} \qquad (B.8b)$$

$$r_{near}=0.5*e^{\frac{2.37-M_w}{\ln(V_{s,30})}} \qquad (B.8c)$$

$$r_{far}=85*e^{\frac{0.4*M_w}{\sqrt{\ln(V_{s,30})}}} \qquad (B.8d)$$